Tech. Rep. CMPSCI-2007-061: Design and Simulation of Minimal Infrastructure Short-Range Radar Networks

Brian C. Donovan
and David J. McLaughlin
Electrical and Computer Engineering Department
University of Massachusetts Amherst
Amherst, Massachusetts 01003
Email: bdonovan|mclaughlin@ecs.umass.edu

Michael Zink
and Jim Kurose
Computer Science Department
University of Massachusetts Amherst
Amherst, Massachusetts 01003
Email: zink|kurose@cs.umass.edu

Abstract

Many sensor network studies assume that the energy cost for sensing is negligible compared with the cost of communications or computing. Opportunities exists to deploy sensor networks utilizing active sensors with a high energy cost such as radar. For a node utilizing radar as its primary sensor, the actual sensing procedure is the main power consumer. In the worst case almost 50% of the power is consumed by the sensing procedure, while only 3% is used for communication, the remainder consumed by the computing platform. In this paper we examine a wireless sensor network composed of short range radars used to monitor rainfall. These short-range radar nodes are designed to be deployed as part of an ad-hoc network and to limit their reliance on existing infrastructure. We refer to these networks as "Off-the-Grid" (OTG) weather radar networks. Independence of the wired infrastructure (power or communications) allows OTG networks to be deployed in specific regions where sensing needs are greatest, such as mountain valleys prone to flash-flooding, geographic regions where the infrastructure is susceptible to failure, and underdeveloped regions lacking urban infrastructure. We present a simulative investigation of such an OTG sensor network. We focus on power management and energy harvesting for the network. We use these simulations to demonstrate how geographic location, battery capacity, optimization of power consumption, and node density have an impact on the performance and operational lifetime of such a sensor network. In addition to these simulations, we present the design and implementation of an OTG prototype sensor node. Experiences and data gained from the operation of this node are used as input parameters for the simulations.

I. Introduction

Power management is an important mechanism to extend the lifetime of wireless sensors and the networks they constitute. It has been shown that the combination of power management and energy harvesting can significantly extend the lifetime of wireless sensor networks. Recently, research in the area of power management and energy harvesting has been focused on small, low-power, sensor systems where data communication is the main power consumer. In this paper, we focus on power management and energy harvesting for a sensor system where the actual sensing procedure is the main power consumer. In the worst case almost 50% of the power is consumed by the sensing procedure, while only 3% is used for communication, the remainder is consumed by the computing platform.

In our specific case we are investigating radar sensor networks with the intent to improve severe weather observations. Such radar sensor networks have the potential to improve our ability to observe, understand, forecast, and respond to weather hazards. These Distributed Collaborative Adaptive Sensing (DCAS) networks will map wind, rain, and thermodynamic variables in the lower troposphere and provide real-time data to end users [1]. Our work is an extension of the existing DCAS concept by introducing a minimal infrastructure architecture. Minimal infrastructure in this case means sensor nodes that operate without gridded power and wired network access [2]. We call a sensor network with such characteristics an Off-the-Grid (OTG) network. Such Off-the-Grid characteristics are extremely important in the case of radar sensors, since the location of the sensor has a high impact on the quality of the sensed data. For example, mountains can block the radar beam and prevent the lower atmosphere in valleys behind mountain ranges from being sensed. Sensor nodes that are independent of existing infrastructure can be placed in more optimal locations to prevent the phenomena of radar beam blockage as described above. The price for this location independence is to enable these sensor nodes with energy harvesting and wireless communication means that allow the maximization of their operational lifetime.

In this paper, we present a simulative investigation of such an OTG sensor network. We use these simulations to demonstrate how geographic location, battery capacity, optimization of power consumption, and node density have an impact on the performance and operational lifetime of such a sensor network. In addition to these simulations, we present the design and implementation of an OTG prototype sensor node. Experiences and data gained from the operation of this node are used as input parameters for the simulations.

Results obtained from these simulations show that the design of such a sensor network is highly dependent on its geographical location. In addition, we show that a reduction in space between sensor nodes (while the size of the overall deployment area is kept constant), surprisingly, leads to lower battery levels. Finally, we believe that OTGsim is the first modular sensor network simulator that allows for an easy exchange of components composing the sensor node due to its sub-model design approach.

The remainder of the paper is organized as follows. In Section II we give an overview on the related work in the area of power management and energy harvesting. The OTG radar sensor network concept including a description of the radar sensor prototype is presented in Section III. Section IV gives an overview on the simulator that was created to simulate such a wireless sensor network. The results of a

series of extensive simulations are presented in Section IV-C.

II. Related Work

This work expands upon simulation results initially reported in [3]. Related work in power management in sensor networks may be divided into two categories. The first category, contains work on energy-aware protocols that are solely based on battery level and do not take energy harvesting into account. For example, Wang et al. [4] develop an energy consumption model for wireless sensor networks. Compared to our approach, their model is only focused on the communication subsystem and does not consider power consumption of other components (e.g., sensing and computing) of a sensor node.

The second category, which is more strongly related to our work, is focused on systems that incorporate energy harvesting as an additional power supply [5], [6]. Raghutan et al. [5] identify tradeoffs for the design of a solar energy harvesting module and show the difference of battery-only systems. This investigation leads to design consideration for energy harvesting systems, which are evaluated on the Heliomote system. In contrast to our work, their work is focused on low power embedded systems that consume power in the order of mW. In [7], the authors extend their work on energy harvesting by an algorithm that adapts the duty cycle of a node based on the input of a periodic harvested energy source (e.g., solar power). Vigorito et al. [6] developed an adaptive control of duty cycling for energy-harvesting wireless sensor networks that does not require a model to predict future harvested energy but simply operates on the actual battery level. The adaptive control approach is evaluated by a single sensor node simulation.

Our work is different in a sense that we do not adapt duty cycling to available energy. Our goal in this initial investigation is to study the performance of a specific wireless sensor network in different configurations. For example, we determine the maximum possible duty cycling frequency based on available energy and geographic location. In future work, we plan on implementing the adaptive control mechanism presented in [6] into our sensor nodes to investigate if the duty cycling frequency of the single nodes can be increased.

The deployment of radar as a network of collaborative instruments was introduced by McLaughlin et al. [1]. This work focused on introducing collaborative sensing to the radar sensing paradigm. Pedersen et al. [8] have deployed marine radars as short range weather radar. Our work extends that of [1] and [8] by introducing sensor network concepts such as energy harvesting and wireless networking.

III. Off The Grid Radar

A. OTG Concept

The Off-The-Grid (OTG) radar class combines wireless sensor networks [5], [9]–[11] with the DCAS concept [1]. By employing wireless sensor network techniques such as ad-hoc networking, energy harvesting and dynamic management, an OTG network may minimize its dependence on existing infrastructure.

Ad-hoc networks make use of wireless links to transport data. Nodes are required to forward data from the original source of the data to its final destination. In some networks, computation may be performed as data moves through the network. Ad-hoc networks are often characterized by a minimum amount of user configuration which makes rapid deployment feasible.

Energy harvesting describes a system's ability to develop its power needs from environmental sources rather than infrastructure sources [5]. Power sources for energy harvesting are numerous, however the power requirements of a radar system suggest use of solar photovoltaic panels [12].

Dynamic management refers to a system's ability to adapt to changing conditions. The system may adapt to changes within the system as well as the environment containing the system. In an OTG network the resources within the system, primarily each individual node's sensing, computing, communications and energy resources, will need to be managed to maximize the lifetime of the system. Dynamic management will enable power savings when sensing requirements are reduced or enable the system to re-route data in the event of a node failure.

Utilizing these three techniques, an OTG radar node has capability to:

- source its prime power needs using energy harvesting rather than existing power infrastructure,
- transport its data and control communications via a wireless ad-hoc communications network rather than existing network communication infrastructure, and
- manage its energy consumption by adapting its functionality to the environmental conditions.

These capabilities enable the OTG node to operate independent of existing power and communications infrastructure. In addition an OTG node should be small and light-weight in order to ease deployment.

As envisioned, an OTG network would be capable of being deployed with a minimum of support equipment. Independence from the wired infrastructure would allow OTG networks to be deployed in specific regions where sensing needs are greatest, such as mountain valleys prone to flash-flooding, geographic regions where the infrastructure is susceptible to failure, and underdeveloped regions lacking

established infrastructure. OTG radar systems may be deployed in developing countries or remote areas that do not yet have the power or communication infrastructure to support larger systems. Networks of OTG radars would be suitable for rapid or temporary deployment.

OTG radar nodes will communicate wirelessly with one another by operating as ad-hoc networks, and they would distribute computational functions among various points throughout the network. The individual nodes derive energy from solar panels and therefore OTG networks operate under a constraint of limited energy consumption. By limiting the power consumption to that which the radar is capable of generating environmentally, operating parameters of the node become constrained. These include: the maximum unambiguous range of the radar, volume update time, and computational capabilities.

Power is consumed within the radar node by three functions of the node: sensing, computing, and communicating. Maximizing the lifetime of the sensor network, perhaps at the expense of an individual node, will require balancing trade-offs between these three functions. Appropriate design of energy-aware control algorithms may take advantage of both prior knowledge of the target application and environment as well as dynamic knowledge of the operating environment.

Power management of an OTG node may be accomplished through a number of ways including: the hardware of the nodes may be optimized for power consumption and low power hardware may be combined with software based power management. Software may manage the components of the system, disabling unused components, using the network's knowledge of current environmental conditions. Examples include: putting individual components such as the sensing transmitter or the control computer to sleep, adjusting estimate precision by lengthening or shortening dwell times, and improving minimum sensitivity or coverage range by increasing the pulse length of a pulse compression wave form.[1]

A number of operating modes may be defined, which are selected dependent on the operating environment. The operating parameters are defined according to a set of basic principles:

- Under clear air conditions the primary network and node objective is to generate and store power. Surveillance should be limited to augmentation of existing radar coverage.
- Stored power should be consumed in proportion to the utility of the data to be acquired.
- Complete network knowledge of the storm should be used in optimizing power consumption.

[1]Pulse compression wave forms introduce blind ranges near the radar due to their longer transmission time. These blind ranges may be overcome by introducing two wave forms, one longer, higher energy, for ranges far from the radar, and one shorter, lower energy for ranges close to the radar.

- When possible computation tasks shall be completed remotely from a storm to make use of clear air conditions.
- Sensing performance shall be dynamically adjusted based upon utility of the data.

Adjusting node performance and task may allow system lifetime to be extended to 24 hour operation for weeks at a time using only solar based input. An implicit assumption is that the value of data is not a constant function of time. For example, during a developing storm, high-sensitivity lower-precision data may be of greater value than low-sensitivity high-precision data. Likewise during periods of high rainfall intensities, where the minimum expected reflectivity is higher, sensitivity may be sacrificed.

To illustrate these concepts, five operational modes for a rain surveillance radar will be considered:

General Surveillance: In general surveillance the individual nodes objective is to harvest a greater amount of energy than is consumed through operations. Once maximum energy storage has been reached, all energy harvested may be utilized immediately or will be lost. Volume coverage pattern (VCP) in this mode would be designed to complement existing WSR-88D coverage on an individual node basis. Volume updates would occur at sparse intervals, for example every 15 minutes, to maximize energy harvesting.

Rain Watch: Nodes may enter a rain watch mode when notified by a neighbor that a rain event is moving toward the node. The node objective is to balance energy harvesting with consumption. Volume update times would be increased, $\sim$ 10 minutes. Sensitivity would be increased to sense low dBZ reflectivity, $\sim$ 20 dBZ. Dwell times would not be increased therefore limiting the precision of the estimates, $\sim$ 3 dB.

Rain Surveillance: When rain is present in the observation domain of a node it would enter the rain surveillance mode. Nodes in this mode would focus on high resolution, low standard deviation rainfall estimates. Nodes would be allowed to consume energy from battery storage. Volume coverage would focus on base reflectivity, allowing dwell times to be increased to improve estimate precision, $\sim$ 1 dB.

Computation & Communications: While in general surveillance mode, nodes could offer computation and communications resources to the network. Network computation such as multi-sensor data fusion, response to user queries or network optimization would be pushed to nodes operating in general surveillance mode. Migrating computation and communications to nodes with greater energy resources could reduce the energy requirements for nodes actively sensing.

Network Sink: The function of the network sink is to provide an interface between the OTG network and an established network infrastructure. The sink requires access to the infrastructure via a wired or

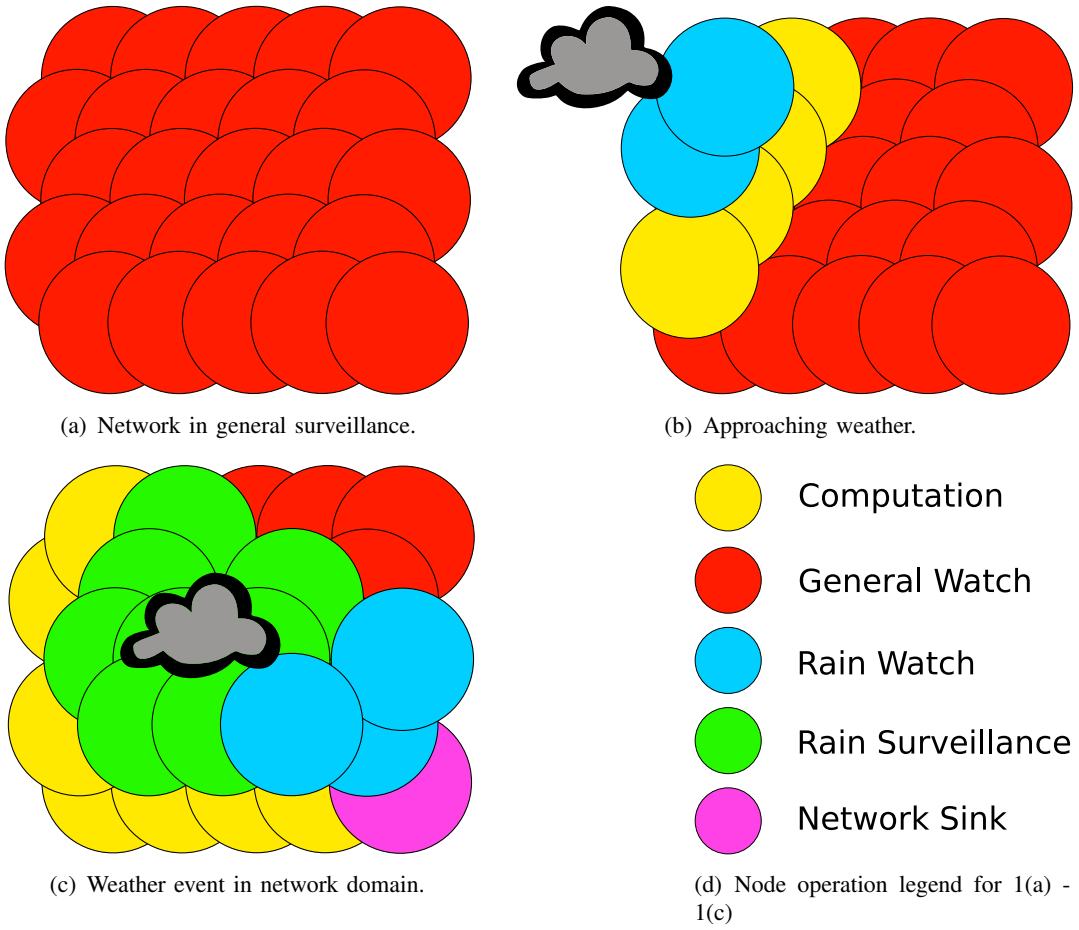

(a) Network in general surveillance.

(b) Approaching weather.

(c) Weather event in network domain.

(d) Node operation legend for 1(a) - 1(c)

Fig. 1. OTG network operation model.

wireless connection. Control requests from end-users may be directed to the sink which would disseminate them through the OTG network. All data for consumption outside of the OTG network would pass through a node operating as a network sink. While end-users may connect to individual nodes in an OTG network via the wireless interface, a sink could be used to provide a public gateway to an OTG network.

Figure 1 illustrates an example time evolution of an OTG network. In Figure 1(a), the network nodes are in the *General Surveillance* mode. In panel b, a new storm event is detected. This detection may have been from the local NEXRAD, via a network sink, or from OTG nodes in the general surveillance mode. Following detection, nodes in the predicted path of the storm cell (estimated using in-network computation of a storm tracking algorithm) enter the *Rain Watch* mode looking for low rain rate precipitation (Figure 1(b)). As the storm cell moves across individual nodes they are placed into *Rain Surveillance* modes, additional nodes are placed into computation mode to accomplish network processing and to forward data (Figure 1(c)). As the storm area or complexity increases the network adapts itself by

distributing computation away from the nodes that are acquiring data. Data is forwarded to the enduser via the *Network Sink*. Following the storm event nodes return to the *General Surveillance* mode.

By taking advantage of the spatial variation within the storm environment, network computation and communications may be completed by nodes not needed for sensing of the storm. By distributing power loads throughout the network, by moving tasks such as scanning or algorithm computation to neighboring nodes, the average power consumption of individual nodes may be lowered. However, distributing these tasks may increase the amount of network traffic moving data between nodes increasing the cost of computation and communications. Simulation of these tradeoffs is studied in Section IV.

B. OTG Node Prototype

The purpose of the OTG Prototype is to provide a demonstration of an OTG class node to inform simulations of an OTG network and to provide a platform for experimentation. The experience gained using the node and measurements of its performance have been used to model the network scale simulation of an OTG system, this is presented in Section IV. This subsection will document the prototype which has been developed and deployed.

1) Prototype Design: Figure 2 presents a block diagram of the general hardware architecture of the prototype node. The four major subcomponents of the system are: the solar power generation, computing, radar, and communication subsystems. The solar power generation subsystem is composed of a solar panel, a maximum power point tracker (MPPT), a deep-cycle battery, and a battery charger. The computing subsystem uses a lower power embedded computer and integrates with the sensing subsystem using a PCI analog to digital convertor (ADC) and a USB based control interface. The sensing subsystem is composed of a commercial marine radar which has been modified to allow for integration with the remainder of the system. The communication system uses a PCMCIA 802.11b/g (WiFi) wireless card and an external directional antenna to provide communications between nodes. Figure 3 shows a picture of the fully integrated prototype node. The electronics box contains all components excluding: the radar, solar panel, battery and WiFi antenna (Figure 4).

The node is built around a 12 V power bus provided by the MPPT. The MPPT regulates power generation from the solar panel and storage in the battery. The battery charger is included to charge the battery or provide 12 V when infrastructure power is available. The 12 V bus powers both the embedded PC and the radar. The radar is powered through the USB interface card which allows the radar power to be switched

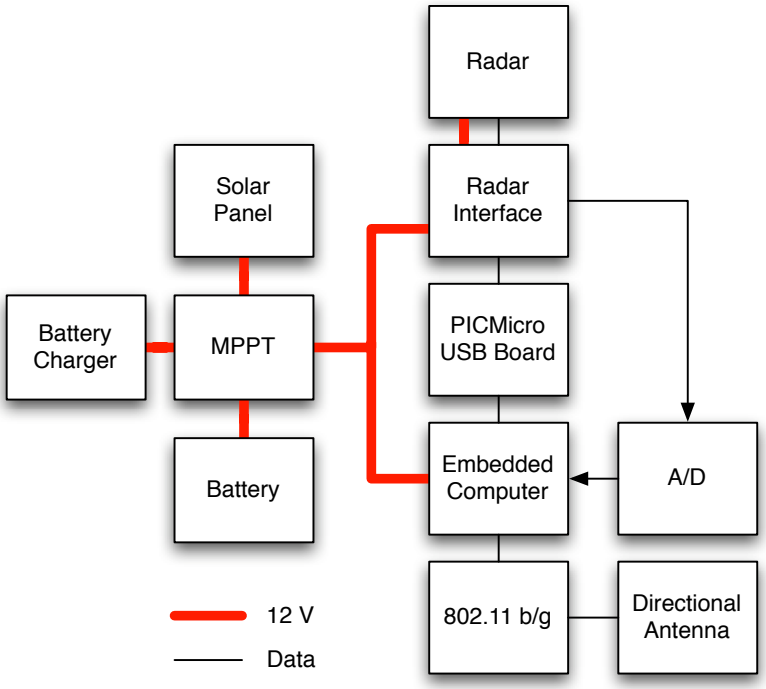

Fig. 2. OTG prototype hardware architecture.

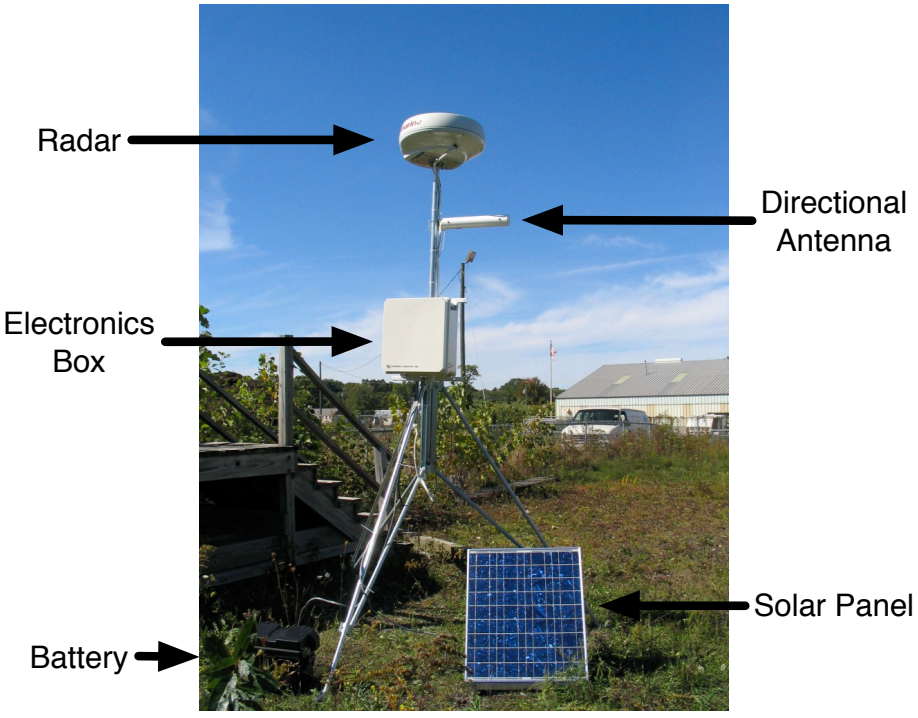

Fig. 3. OTG prototype node.

Fig. 4. OTG prototype electronics box.

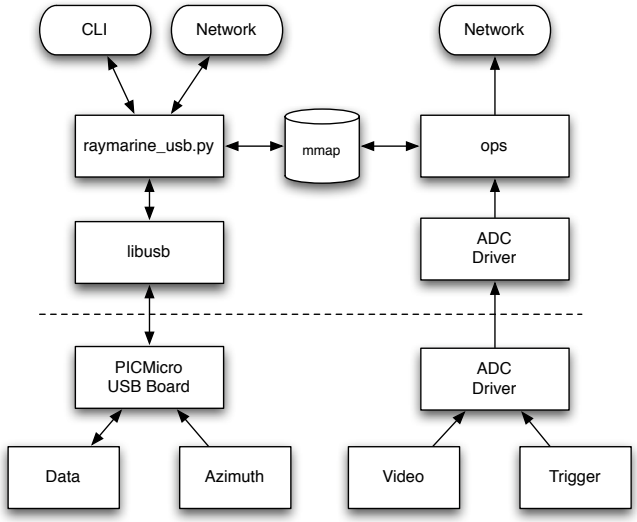

Fig. 5. OTG prototype software architecture with hardware interface. The dashed line separates software (above) from hardware (below).

under computer control.

The USB interface board is composed of a PIC® micro-controller, providing the USB interface, and a custom printed circuit board (PCB) interfacing with the radar. The radar interface is a 4 pair connection composed of: data, trigger, antenna and video signals. The data, trigger, and antenna signals are RS-422 serial connections. The video is the analog output of the log detector located in the radar receiver. The data connection is driven by the micro-controller and provides bi-directional communication with the radar. The trigger and video signals are fed to the ADC by coaxial cables. The antenna position signal is a 820 Hz pulse which is counted by the micro-controller to provide antenna position estimates.

Figure 5 presents the software architecture for the prototype node. Two main processes manage the input and output of data from the radar. One process (*raymarine_usb.py*) accepts control input from a command line interface or over the network via remote procedure call. The process then controls the radar via the USB interface using the appropriate radar serial commands read from a text file. The control process communicates with the data acquisition process (*ops*) via a memory mapped file. The *ops* process controls the sampling of the radar video signal and outputs data directly to the network via a socket. Data is not written locally to the node for long term storage.

2) Power Consumption: A breakdown of the prototype power consumption has been used to model the node for simulation. This section presents the power breakdown for the major functions of the OTG prototype.

Power is consumed in the radar by the electronics required to control the radar, the motor rotating the antenna and the high power pulse generating magnetron. In standby mode the electronics and magnetron heater are active while the antenna is not rotating. When the radar is transmitting the antenna is rotating and the magnetron is firing.

In addition to the radar, power will be consumed by the computation and communication functions of the OTG node. The computation function is composed by three main components: the motherboard [13], the PCI ADC card [14], and a compact flash card. The power consumption for computation is comparable to that of the sensing function. If the sensing function is not being used the ADC would not be required reducing the power consumption of the computation system by 40%.

The final function of an OTG node is the communications function. The OTG prototype uses 802.11b/g for point-to-point wireless communications. A PCMCIA wireless card is paired with a passive directional antenna in order to achieve long distance communications ($\sim$ 10 km). The wireless card currently being used draws approximately 2W when transmitting and 1.4W when receiving [15].

Table I presents the empirical worst-case power consumption of each of the three functions of the node. The data in this table was measured at the 12 V bus supplying the complete node. The power consumption was measured as each function was enabled.

3) Deployment: Two OTG prototype nodes have been deployed in Western Massachusetts as part of an OTG technology testbed. An additional two sites are currently planned for expansion of the network. The location of these four sites are show in Figure 6. The currently deployed OTG systems (Figure 7)

TABLE I
EMPIRICAL OTG PROTOTYPE POWER BREAKDOWNS (W)

Sensing			Computation			Node	
Heater & Controller	10		Motherboard	17		Sensing	34
Motor / Inefficiencies	21		A/D	13		Computation	33
Average Radiated Power	3		Storage	3		Communications	2
Total	34		Total	33		Total	69

have been installed on preexisting towers (Figure 8). The University of Massachusetts (UMass) Orchard Hill tower hosts a CASA IP1 class radar referred to as the MA1 radar. The Mt. Toby installation is hosted on a Massachusetts Department of Conservation and Recreation fire tower. An 802.11 b/g wireless communications link has been established between the OTG located on the Orchard Hill tower (the OTG node is referred to as MA2) and the Mt. Toby OTG node. Communications for the MA2 radar is provided by the Orchard Hill tower communications infrastructure which connects the testbed to the public internet. Data from both the Mt. Toby and MA2 OTG nodes may be relayed over the public internet to data archive servers on the UMass campus.

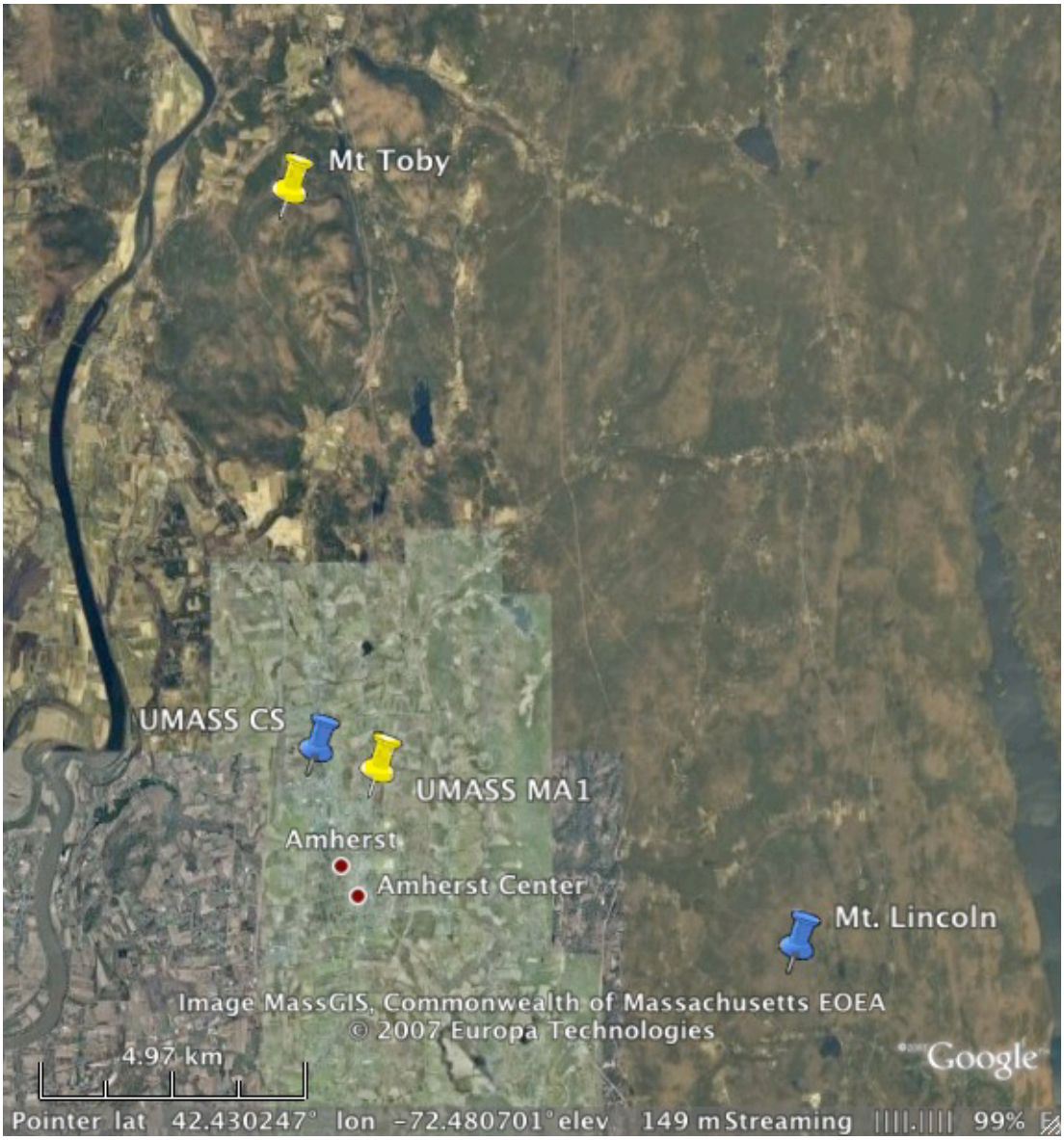

Fig. 6. Location of current (yellow) and planned (blue) OTG radar deployments as part of CASA Massachusetts OTG Technology Testbed. Distance from Mt. Toby to UMass MA1 is approximately 10.8 km, UMass MA1 to Mt. Lincoln, 8.3 km, Mt. Lincoln to Mt. Toby 16.6 km, UMass CS to UMass MA1, 1.2 km.

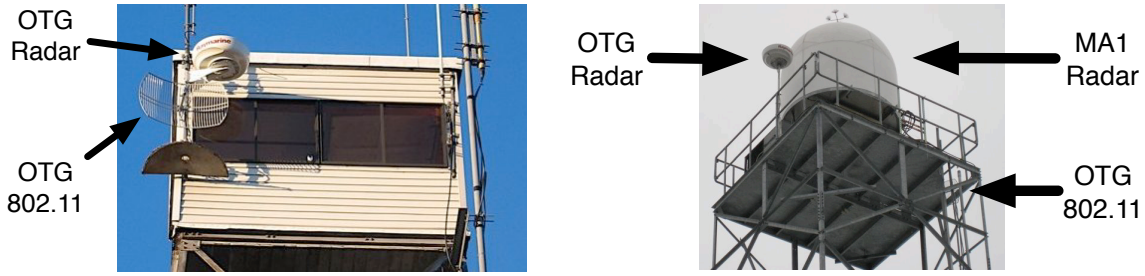

(a) Mt. Toby (b) UMass Orchard Hill

Fig. 7. Detail of deployed OTG nodes in Western Massachusetts technology testbed.

(a) Mt. Toby

(b) UMass Orchard Hill

Fig. 8. Installation sites of deployed OTG nodes in Western Massachusetts technology testbed.

IV. Network Simulation

A network simulator, *OTGsim*, has been developed to study potential OTG networks. OTGsim is a discrete time simulator that models networks of OTG nodes and their communications. Simulation of OTG networks enables experimentation with the OTG concept without the expense of a full OTG network deployment. Networks of tens to hundreds of OTG nodes may be simulated to study the impact of: network location, node spacing, data routing, and control decisions. Simultaneously the deployment of small scale OTG networks will enable the validation and refinement of the OTG simulator.

The OTG simulator provides a general framework which may be developed to extend the models to other high-energy sensor types. Modules of the simulator may be replaced individually to study alternative control schemes, sensor systems (LIDAR or more advanced RADAR) and power generation. Here the OTGsim is used to study networks composed of nodes similar to the OTG prototype described in Section III-B. This section will present the design of the OTGsim simulator and a series of experiments exploring fixed design time parameters of the nodes and fixed interval scanning.

A. OTG Network Simulator

The OTG simulator is built using the SimPy discrete simulation package [17]. The software architecture of the OTG simulator is presented in Figure 9. During a simulation run a network topology consisting of one or more nodes is created. Every node is composed of sub-models for each of four subsystems: sensing, computing, communicating and power generation. The sub-models report their energy consumption or generation to an energy aware control module. A network definition file is used to describe the node's locations and the network links between nodes.

Two external data sources are used to drive the simulations. The U.S. National Renewable Energy Laboratory's Typical Meteorological Year 2 (TMY2) data set [18] is used to drive the estimation of solar power generation. NEXRAD data from the National Climatic Data Center Data Archive [19] is used to simulate "workloads" for the network. The archive data may be used to simulate the data that each radar in the network would observe. This may be used to evaluate dynamic control, network routing and data compression algorithms specific to the weather radar application. These data files and their use in the simulator are documented in the Appendix.

The power sub-model models a fixed tilt solar panel of a specified area. The solar power incident on

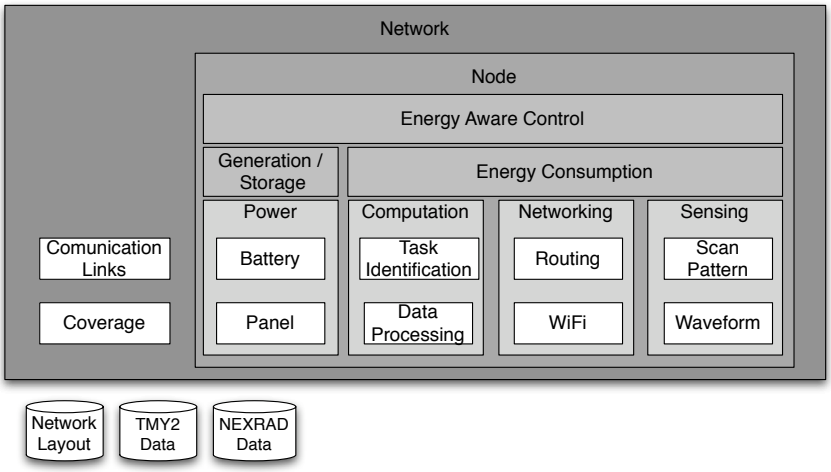

Fig. 9. OTG simulator block diagram.

the panel is estimated from the TMY2 data set using the procedure in the Appendix. The effect of panel tilt, area and efficiency as well as snow cover are included in the estimation. Simplified, the estimated power output of the panel is,

$$P = eI_T = eI\left(\theta, \beta, \rho_g, t\right) \tag{1}$$

where P is the power generated by the panel, e the efficiency of the panel, and I_T the total radiation incident on the panel. The total radiation incident on the panel is a function of the panel's latitude (θ), tilt (β), the reflectance of the ground (ρ_g) as estimated by the snow cover, and the solar time t. In these simulations the solar panel was vertically tilted at an angle equal to the latitude of the node and facing due south, the power optimal directions for a fixed tilt solar panel in the northern hemisphere [20]. The full expression for the total radiation incident on the panel, Equation 11, and its derivation are presented in the Appendix. If a NEXRAD data set is used to drive the simulation the incident solar power is set to zero if there is positive reflectivity (indicative of rain) in the node's coverage area. Power generated by the panel is stored in the battery model.

The computation sub-model generates tasks for the energy aware control to select from. It also includes both the radar control and network routing algorithms. The radar control issues *radar scan* tasks which may be generated at fixed time intervals or based on the weather environment. Different control schemes may be tested by replacing this module. The network routing control implements the distance vector routing algorithm [21] to create network routes for each node. The routing control operates by issuing

network *send* and *receive* tasks to the energy aware control.

The networking model simulates a simplified networking stack. It assumes: (a) a reliable networking paradigm where messages may be passed between nodes, and (b) a physical link provided by 802.11 b/g hardware operating at the maximum fixed speed, 8 Mbps, observed in simulated tests [22]. Energy consumption is estimated on a per message basis, based on the message size in bytes, the transfer speed and the energy consumption of the networking card. Transfers proceed if both the sender and the receiver have sufficient energy, otherwise the message is buffered at the sender. For the simulations an unlimited buffer size is assumed.

The radar model estimates the energy consumption required to sample the atmosphere. The energy consumption is estimated from the total transmit time of the scanner and the energy consumption rate of the transmitter. If NEXRAD data is available the data is "sampled" to an azimuth-range array based on the beamwidth characteristics of the simulated antenna. The sampled data is then passed to energy aware control for further computation or transmission. The default radar scan pattern is a 360° azimuth scan at 0° elevation over 30 seconds.

Validation: The OTG technology testbed described in Section III-B3 will be used to refine and validate OTGsim. The sub-models energy consumption parameters are based on the measured power consumption of the individual OTG prototype components listed in Table I. As the TMY2 dataset is based on a 30-year average of historical data it is not possible to directly validate the results of the simulations run with the TMY2 dataset. The interface PCB used in the OTG radars has been modified to allow for the measurement of current draw while the nodes are in operation. This measurements will allow for the inter-comparision between the performance of the testbed and simulation runs using the current profile generated by the solar panel. As the size of the OTG testbed expands measurements taken of current consumption will be used to refine the sub-models used in the simulator and validate the simulations against the operation of the network.

B. Network Topology Generator

The OTG networks used in the following experiments were generated automatically from user defined seed sites using a desired range between nodes. Line of sight between nodes is estimated using United States Geological Survey (USGS) 1° Digital Elevation Maps [23], [24] to determine communication links between nodes. Network node locations are generated using Algorithm 1. New nodes are added to

the network in multiple rounds. Starting with each existing node (seed nodes in first round), potential locations are generated around the node in a circle with the desired radius. Potential nodes are eliminated by limiting overlap with existing nodes to the desired range and requiring a line-of-sight to at least one existing node. The remaining nodes are filtered to maximize distance and the number of line-of-sight links between nodes. The nodes that remain after filtering are added to the network and the process repeats until the user-defined area has been covered. The result is a fully connected network of nodes satisfying line-of-sight communications (excluding trees and man made structures).

Figure 10 illustrates six potential OTG network deployments generated using Algorithm 1. The figure indicates the locations of nodes in the network and the line-of-sight communication links between nodes. These networks were generated based on the terrain in western Massachusetts near the University of Massachusetts Amherst. The USGS DEM used in the generation is shown in Figure 12. Networks were generated with node spacing from 5 to 30 km. Figure 11 presents the line-of-sight coverage at 100 m elevation for each of the networks. The radar range has been limited to the node spacing. As would be expected the 5 km spacing has better coverage than the longer spacings. The longer ranges are limited by the line of sight requirement which prevents coverage in some locations.

These hypothetical networks will be used to simulate OTG network performance.

Algorithm 1 Network node location selection.

```
Require: q: a queue of points to be examined
Require: d: desired distance between nodes
  while q is not empty do
    p ← q.get()
    if p has explicit transmit height then
      tx_height ← p.tx_height
    else
      tx_height ← default height
    end if
    rx_height ← default height
    candidate_points ← empty array
    for angle = 0 to 360 do
      generate a new point at distance dist
      test distance
      test line of sight to count number of links
      reject if there is no LOS to existing radars
      reject if we are to close (.75 * dist < d < dist + 1.0 ) to other radars
    end for
    sort candidates by maximum number of los links
    while canidate_points.length > 0 and current_los_links > 0 do
      priority_points = x for x in canidate_points if current_los
      sort based by node elevation
      remove all points not equal to maximum node elevation
      sort for max distance from other nodes
      select node with maximum distance from other nodes
      append selection to q
      remove points within dist - 1 of selection from canidates
    end while
  end while
```

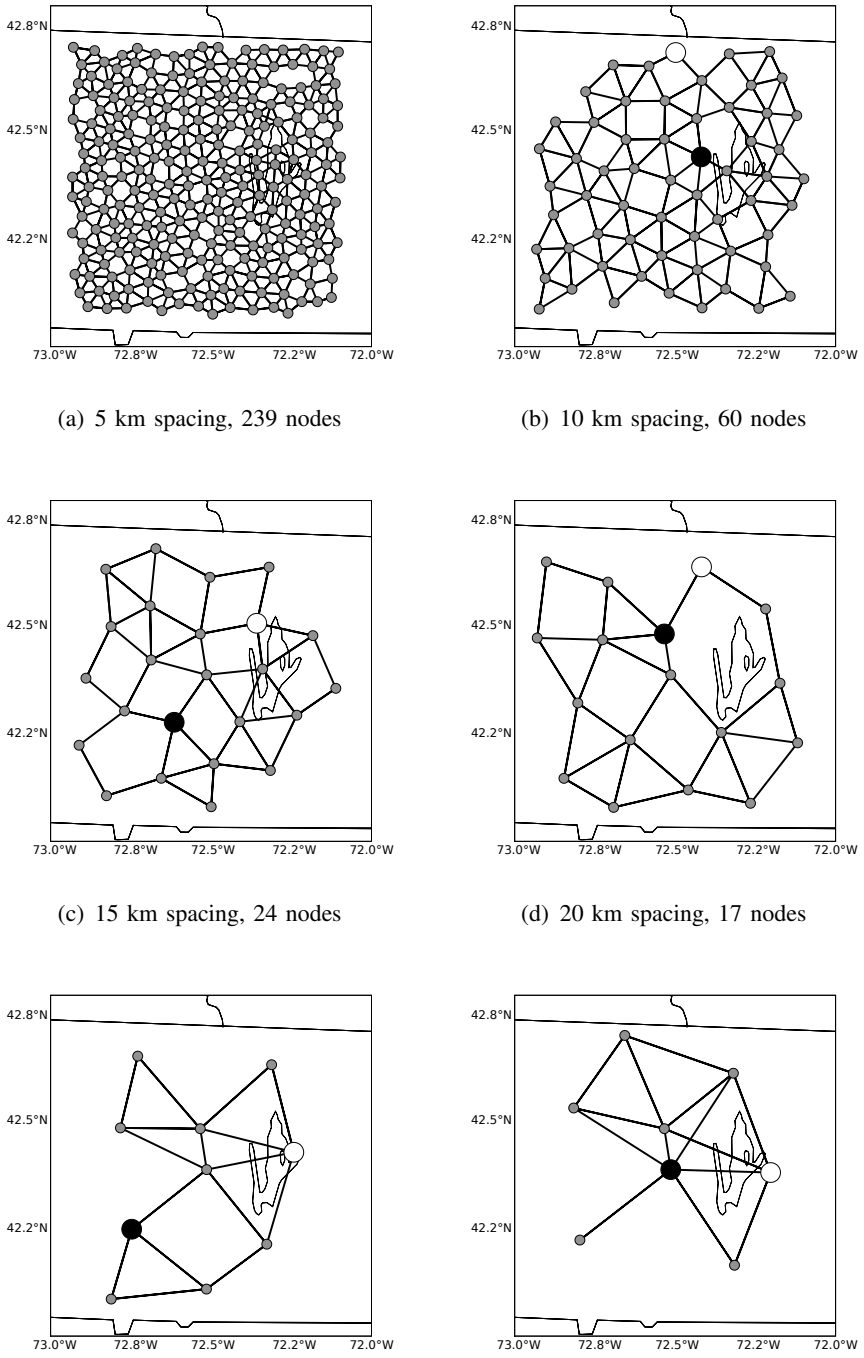

(a) 5 km spacing, 239 nodes

(b) 10 km spacing, 60 nodes

(c) 15 km spacing, 24 nodes

(d) 20 km spacing, 17 nodes

(e) 25 km spacing, 10 nodes

(f) 30 km spacing, 8 nodes

Fig. 10. Example networks for simulation. Dots indicate node location. White and black dots indicate nodes with minimum and maximum cumulative battery level as discussed in Section IV-E. Black lines indicate line of site communications link. Domain is located in Western Massachusetts. The outlined shape in the maps is the Quabbin Reservoir near Belchertown, MA.

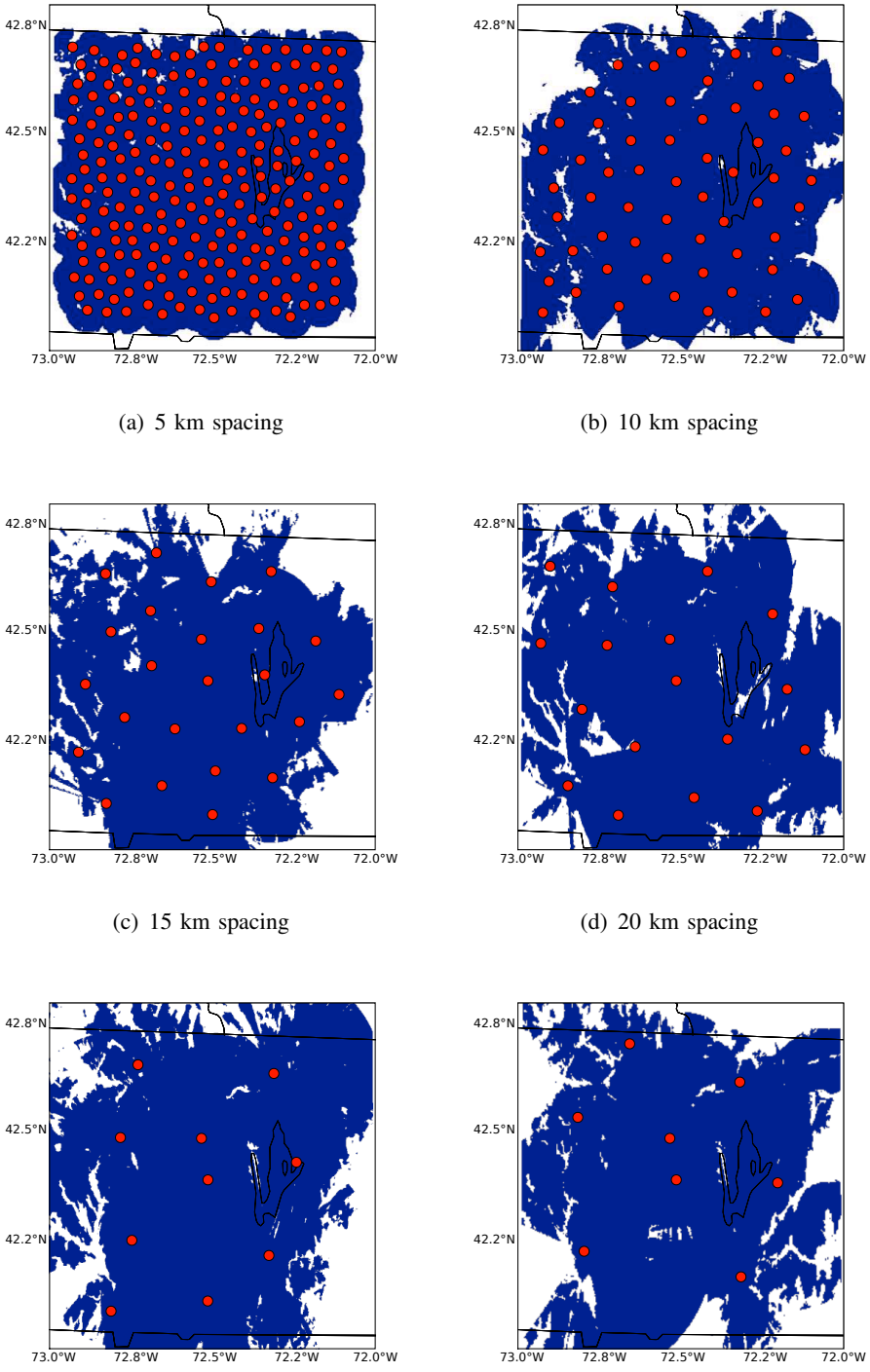

(a) 5 km spacing

(b) 10 km spacing

(c) 15 km spacing

(d) 20 km spacing

(e) 25 km spacing

(f) 30 km spacing

Fig. 11. OTG network line-of-sight to 100 meters above ground level for six network spacings $R \in [5, 10, 15, 20, 25, 30]$. Networks (Shown in Figure 10) located in western massachusetts. Red dots indicate node location.

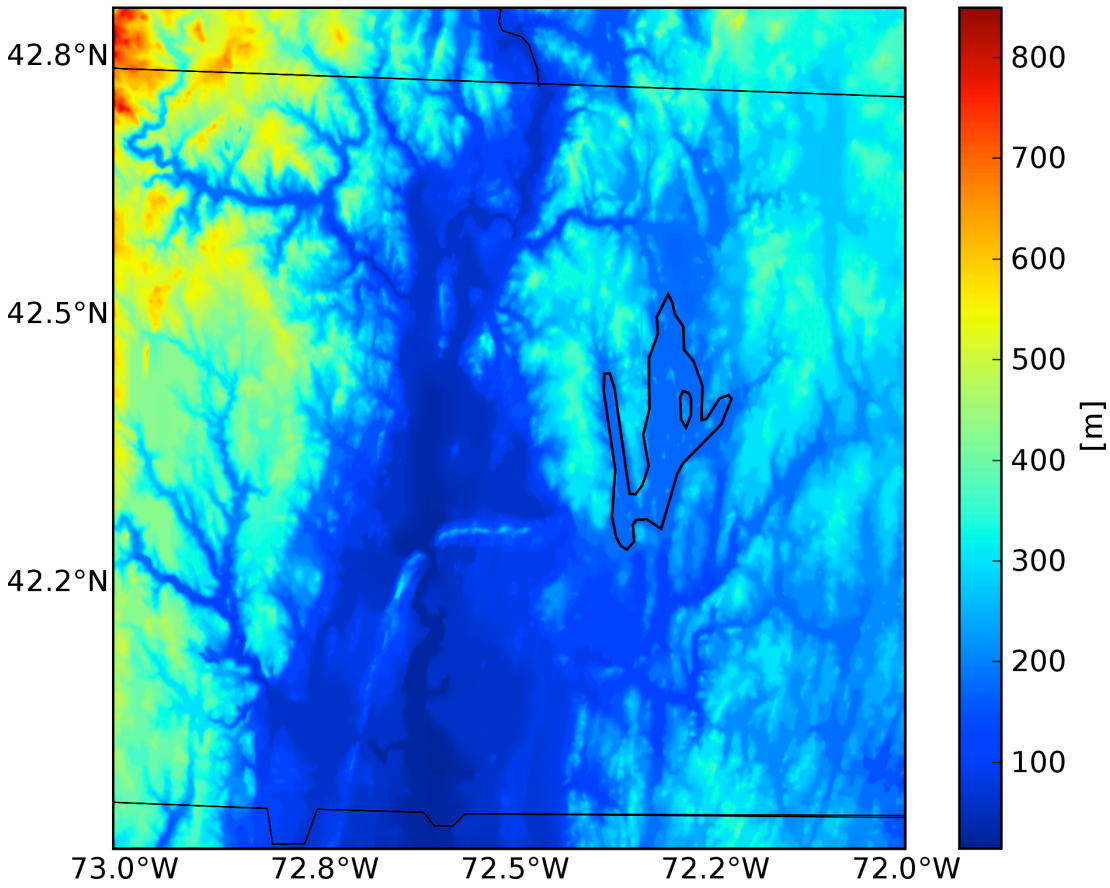

Fig. 12. Western Massachusetts USGS Digital Elevation Model used to generated networks shown in Figure 10.

C. Experiments

A number of experiments were performed using the OTG simulator to explore the performance of an OTG sensor network as it is described in Section III. The primary metric examined is the battery level of the individual nodes. If the battery level drops to 0% the node will fail due to lack of power. All of these experiments were simulated with a 60 second time resolution.

This section presents the result of a number of simulation experiments using the OTG simulator. Section IV-C1 presents the variation in generated power due to the geographic location of the network. Section IV-C2 evaluates the impact of the solar panel and battery on extending lifetime performance. Section IV-D considers the potential power optimization of the sensing and computing platforms composing the node. Finally, Section IV-E evaluates the impact of node separation.

1) Geographical Location: The first experiment examines the impact of the variation in solar input due to geography. In this experiment OTG nodes were simulated in 6 locations across the United States and Puerto Rico. The simulation sites are listed in Table II and shown in Figure 13. The goal of this experiment is to show how much energy can be created by a single OTG node based on its geographical location.

In this simulation each OTG node is outfitted with a southward facing 0.5 m^2 solar panel tilted at an angle equal to the latitude of the node. Each location was simulated for 18 months with an empty battery at the initialization of the simulation. Daily solar generation for each of the six sites is shown in Figure 14 in Watt-hours (Wh) for the first 12 months[2]. The estimated solar power is based on the TMY2 data set with an assumed panel efficiency of 14%.

In general, the peak daily solar power generation for all six sites is between 500 and 600 Wh. The minimum daily generation falls below 100 Wh for the northern sites (WA and WM) while the more southerly sites have more narrow ranges between minimum and maximum generation. The trend in generated solar power becomes more apparent when the mean daily solar generation is averaged to monthly intervals, as shown in the Figure 15. The northerly sites (WM,WA) suffer from severe reduction in available power during winter months. This limits the ability of such sensor networks to survive during winter months in those locations. A functioning radar sensor network at these locations is crucial due to the threat of winter storms.

[2]Daily solar generation for the last six months of the simulations is equal to that of the first six months.

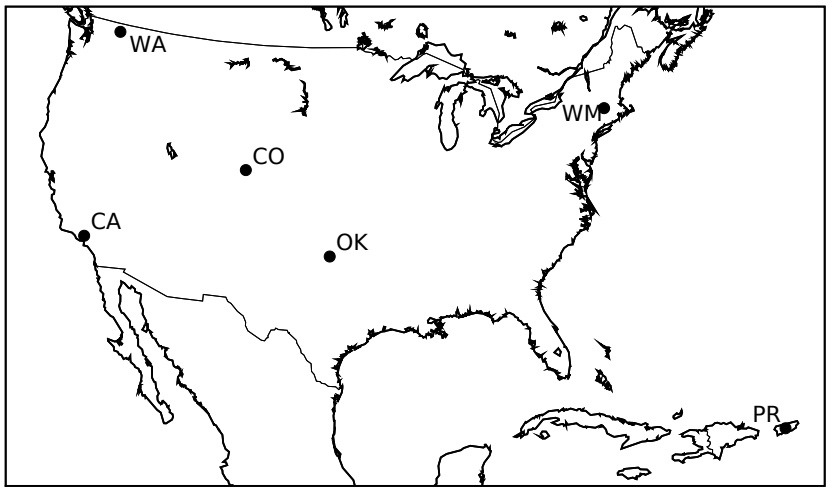

Fig. 13. Location of simulation sites used in the geographical location experiment. Site locations are listed in Table II.

Site	Latitude	Longitude
WM	42.392 N	72.517 W
OK	34.839 N	98.103 W
CO	40.497 N	105.639 W
CA	34.390 N	118.539 W
PR	18.200 N	66.528 W
WA	48.447 N	119.474 W

TABLE II
LATITUDE AND LONGITUDE OF LOCATION EXPERIMENT SITES SHOW IN FIGURE 13.

2) Battery Capacity and Panel Area: In this simulation, the nodes making up the networks are based on the prototype described in Section III-B. The radars were operated with a fixed interval scan pattern. The radar scans its volume for 30 seconds and then "sleeps" for 5, 10 or 15 minutes. It was assumed that the radar does not draw any power while sleeping and does not require any time to wake from sleep. This assumption neglects the boot time and energy draw during times when the CPU is not active but the memory continues to draw power. Therefore, the results presented here may be considered the best case scenario for power consumption.

It was also assumed that the radar nodes can be woken up via remote signaling over the wireless network if sufficient power is available at the receiving node. In the following, we study the performance of an OTG radar sensor network based on battery level. The battery level was used as a measure to compare the performance of different configurations of the OTG network at different locations. For this simulation two battery scenarios were considered: (1) the battery had infinite capacity, and (2) the battery

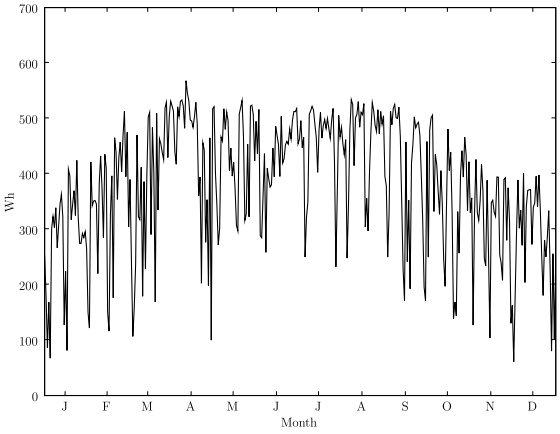

(a) CA

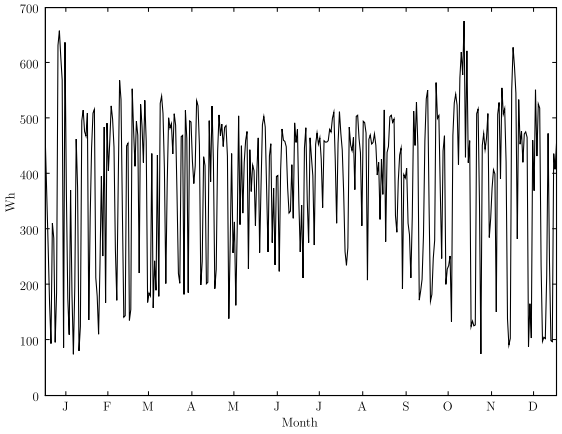

(b) OK

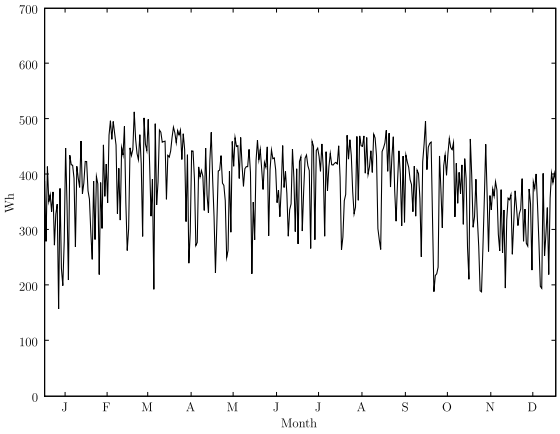

(c) PR

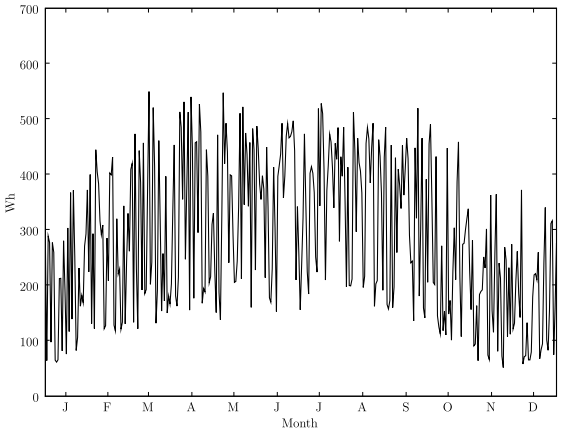

(d) WM

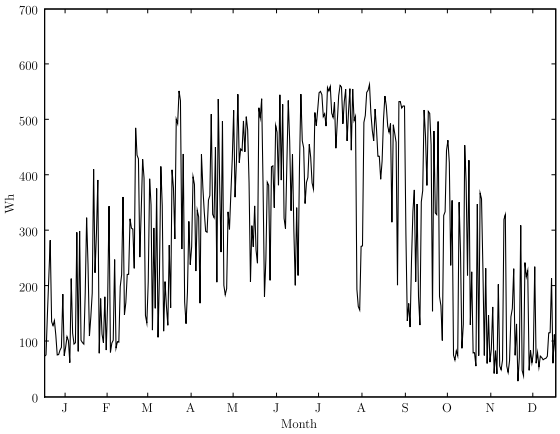

(e) WA

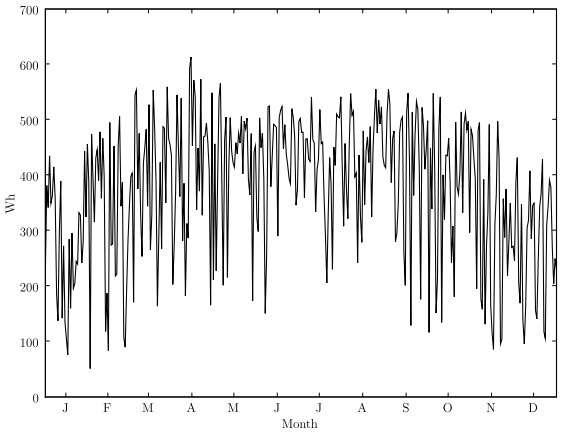

(f) CO

Fig. 14. Daily estimated solar power generation for the six sites in the location experiment.

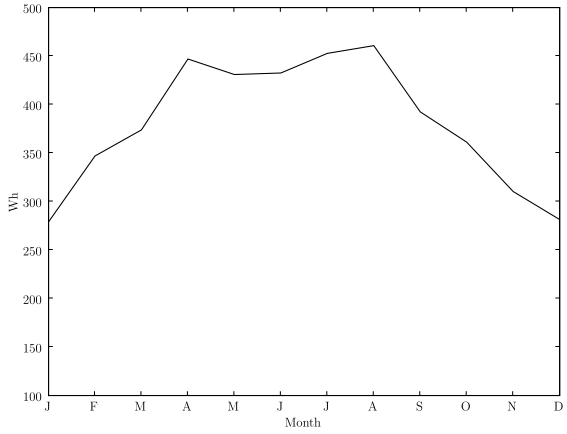

(a) CA

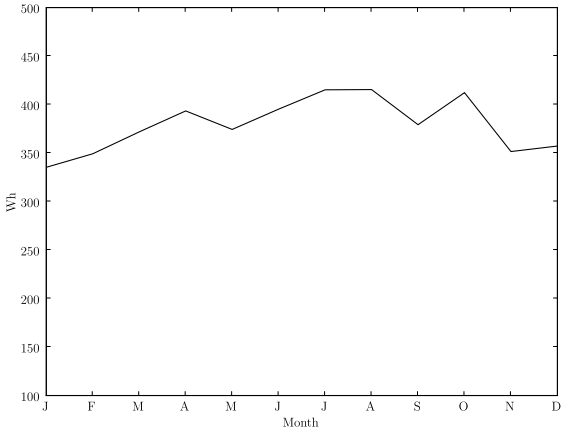

(b) OK

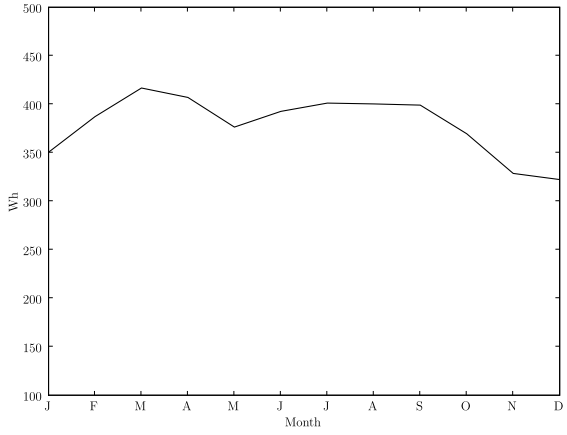

(c) PR

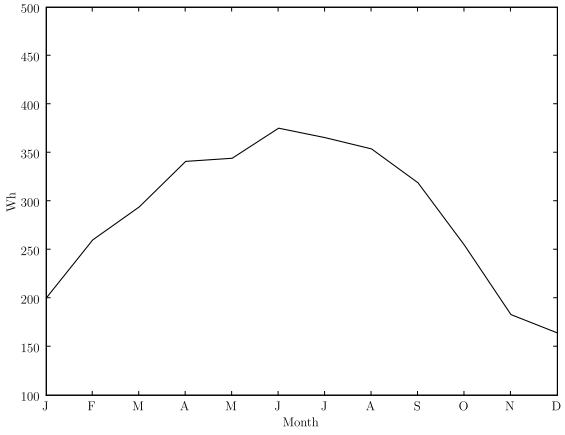

(d) WM

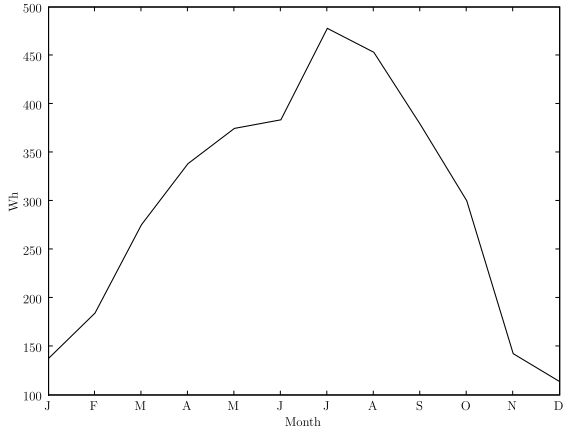

(e) WA

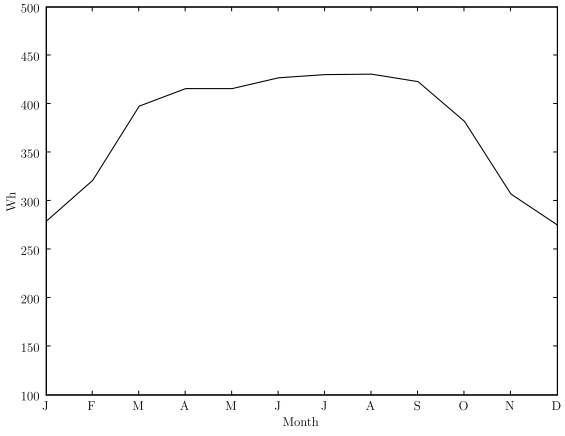

(f) CO

Fig. 15. Mean daily estimated solar power generation by month for the six sites in the location experiment.

capacity was limited to 110 Ah. In each case the battery was completely empty at the beginning of the simulation. Both scenarios use networks with 30 km node spacing between radars. An example network topology for the Western Massachusetts location is shown in Figure 10(f). Data created at the nodes is forwarded - according to routes determined by the distance vector routing protocol - to the seed site at the center of the network, which represents the data sink.

Unlimited Battery: During the first experiment the battery associated with each node was allowed to store an unlimited amount of energy. In this scenario, it is possible to determine if the node is limited by the solar power generated or if it is limited by the battery's capacity. Figure 16 presents the battery level at each site for the 5, 10 and 15 minute sleeping times of the radar. The battery level is presented in units of percent capacity of a 110 Ah battery. This is the same battery size used in the prototype and in the limited battery experiment (see Section IV-C2).

Figure 16 indicates that all of the six locations are capable of supporting year round operation for each of the three scan intervals if an unlimited capacity battery is used. This is indicated by the fact that none of the battery levels returns to 0 after the start of the simulation. Figures 16(f) and 16(e) demonstrate that a large battery will be required for these two locations to buffer the energy loss during the months from October to January where the battery level dips as more power is consumed than is generated.

Figure 17 presents a second unlimited battery experiment in which the panel size was reduced for the Western Massachusetts (WM) and Washington state (WA) sites. Reducing the solar panel in size has an beneficial impact on cost and wind loading. Wind loading is of importance if a node is installed on smaller tower structures like the tripod shown in Figure 3. In this experiment the battery is again unlimited and the panel size was simulated with 0.375, 0.438 and 0.466 m^2 areas while the scan interval remains fixed at 5 minutes. As the figure indicates both locations are unable to support a 5 minute scan interval if the panel is reduced to 0.375 m^2.

The following examines the combination of panel size, load, and available solar input power to determine the required battery capacity. The size of the required battery may be determined from the capacity difference between the two inflection points in each line of Figure 17. For example, for nodes in WA using a 0.438 m^2 panel the battery charge peeks at approximately 1500% and drops to 500% relative to a 110 Ah battery. Therefore a battery with a capacity 10 times the prototype battery, or approximately 1100 Ah would be required to operate the node year round. As the panel size is increased the required

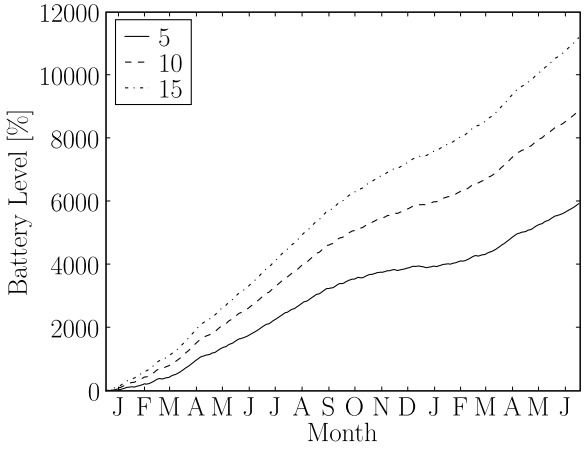

(a) CA

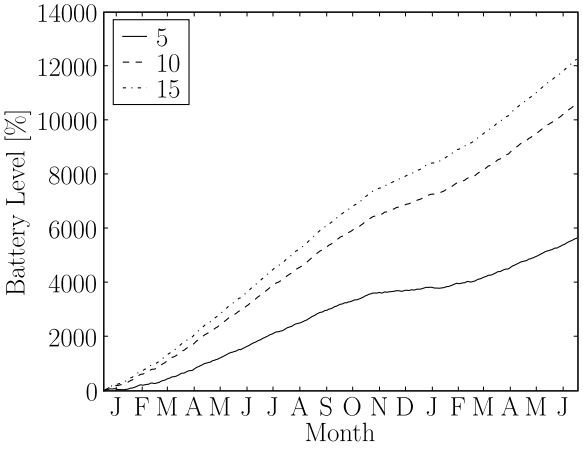

(b) CO

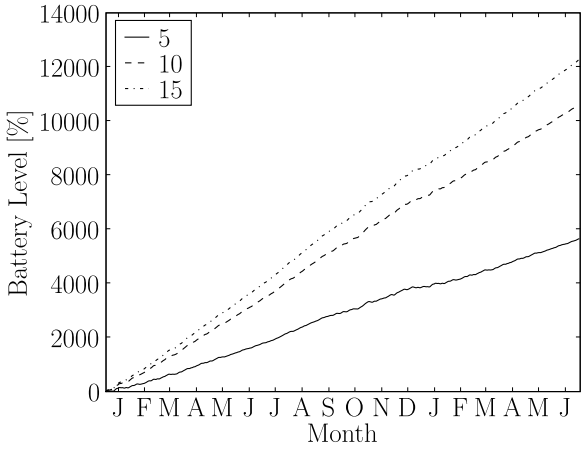

(c) OK

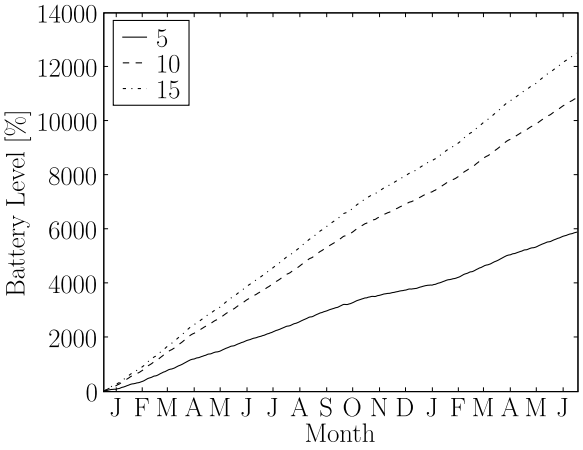

(d) PR

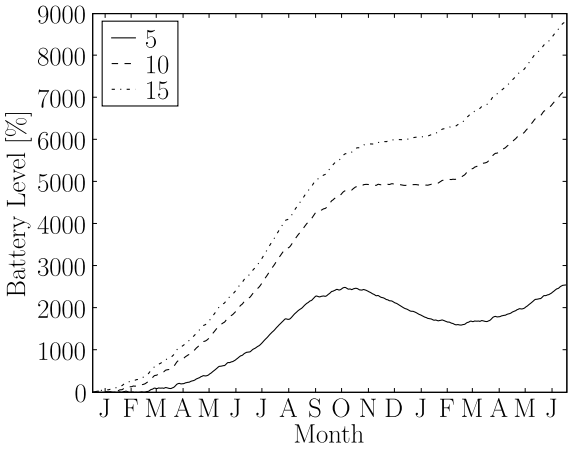

(e) WA

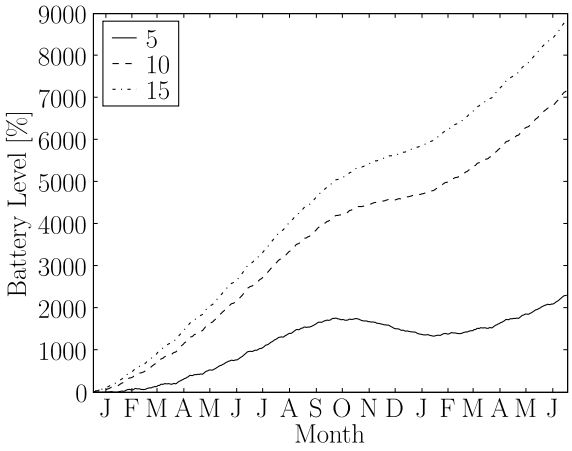

(f) WM

Fig. 16. Unlimited battery experiment: battery level in percentage capacity relative to a 110 Ah battery. Nodes were simulated with an unlimited battery, 0.5 m^2 panel and three different scan interval times: 5, 10 and 15 minutes.

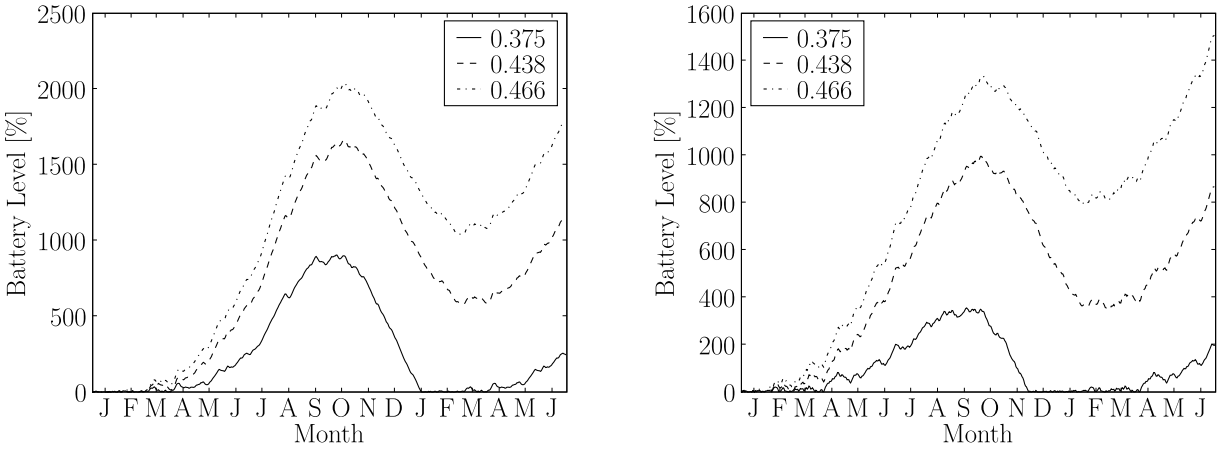

(a) WA (b) WM

Fig. 17. Unlimited battery reduced panel size experiment: battery level in percentage capacity relative to a 110 Ah battery. Nodes were simulated with an unlimited battery using a 5 minute scan interval at three different panel sizes 0.375, 0.438 and 0.466 m^2

battery size is reduced as more energy is produced during the low energy months. For WA a node with a 0.5 m^2 panel would require a battery of approximately 900 Ah. Batteries this large, while possible, are unrealistic for a sensor network deployment because of their high cost and weight.

Limited Battery: In the limited battery experiments the battery capacity of the node is limited to 110 Ah, the same capacity as the prototype. Like the unlimited battery experiments the radars use a fixed interval scan time with a 30 second scan followed by a fixed sleep time of 5, 10 or 15 minutes. Figure 18 presents the battery level over 18 months using the same networks and locations as the unlimited battery experiments. In this experiment the battery constrained networks are WM and WA. In these two locations the nodes were unable to support the 5 minute scan interval. The WM site did not store or generate enough energy to scan between November and mid January while the WA site could not scan between November and mid February. WM and WA were both able to support 10 and 15 minute interval scans year round. The other four sites support all three scan intervals year round.

For the battery limited sites increasing the solar panel or the battery will reduce the time during which the node is unable to scan. Figure 19 shows the results of a second limited battery experiment in which the panel and battery size was increased for both the WM and WA sites while the radar scanned every 5 minutes. In this experiment six combinations of panel (0.4, 0.5 or 0.6m^2) and battery (110 or 220 Ah) were simulated. For the WM site each additional tenth of a meter squared of solar panel extended the operation time by an additional month. When combined with a 220 Ah battery and a 0.6 m^2 panel the

WM site was able to support 5 minute scan intervals. Adjusting panel and battery size had a more limited impact on the WA site. A 220 Ah battery and a 0.6 m^2 panel extended operation by approximately a month but was unable to support full 5 minute scans year round.

D. Optimizing Power Consumption

In addition to increasing the available power by adjusting panel size or battery capacity, node operation time may be extended by reducing the power consumption of the various subsystems. In this experiment the power consumption of the computer and radar were reduced to examine the potential to increase node operation time. Each node was simulated with a 0.5 m^2 panel and a 110 Ah battery. The computer and radar power consumption was varied independently. Each node was simulated with a 5 and 10 Watt reduction from the prototype's power consumption for each sub-system. The nodes used a 5 minute scan interval. The WM site was used for the simulation.

Figure 20 presents the battery level for the reduced consumption systems. In the left column the computer power consumption is fixed while the radar power consumption is varied. In the right hand column the radar power consumption is fixed while the computer consumption is varied. The experiment indicates that reducing the computer consumption has a greater effect on the operation time than the reduction of radar consumption. This is likely due to the greater amount of time that the computer operates as it is on during network operations (transmitting and forwarding data) as well as during the sensing periods.

E. Node Separation

The node spacing experiment examines the impact that separation has on energy consumption. Networks were simulated in two locations, WM, and PR, using separations of 10, 15, 20, 25 and 30 km (exsubsectionample networks for the different separation distances for the WM site are shown in Figure 10 and PR in Figure 22). The coverage area of the network is fixed. As the separation decreases the total number of nodes in the network increases. The range of the radar at each node is set equal to the node spacing. While this implies that each node produces less data, overlap in areas that are scanned by multiple radars may increase thereby increasing the total amount of data collected. Increased overlap with smaller node spacing is caused by an increase in the number of points which may be sampled by more than one radar as the spacial density of the radars is increased.

Figure 23 presents the average battery level across all of the nodes in the network. The reduction in

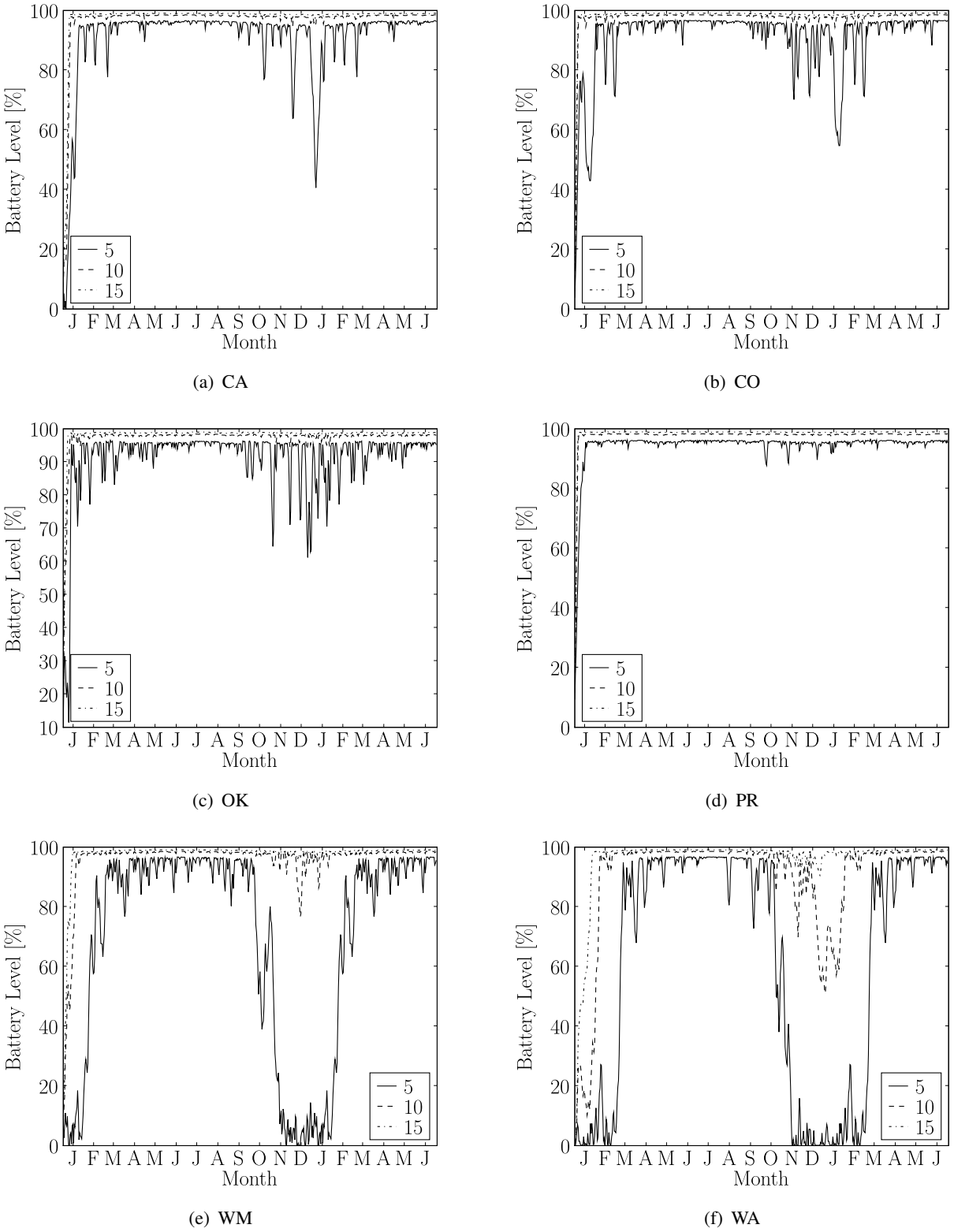

(a) CA

(b) CO

(c) OK

(d) PR

(e) WM

(f) WA

Fig. 18. Limited battery capacity experiment: battery level in percentage capacity relative to a 110 Ah battery for six locations with a fixed 110 Ah battery capacity.

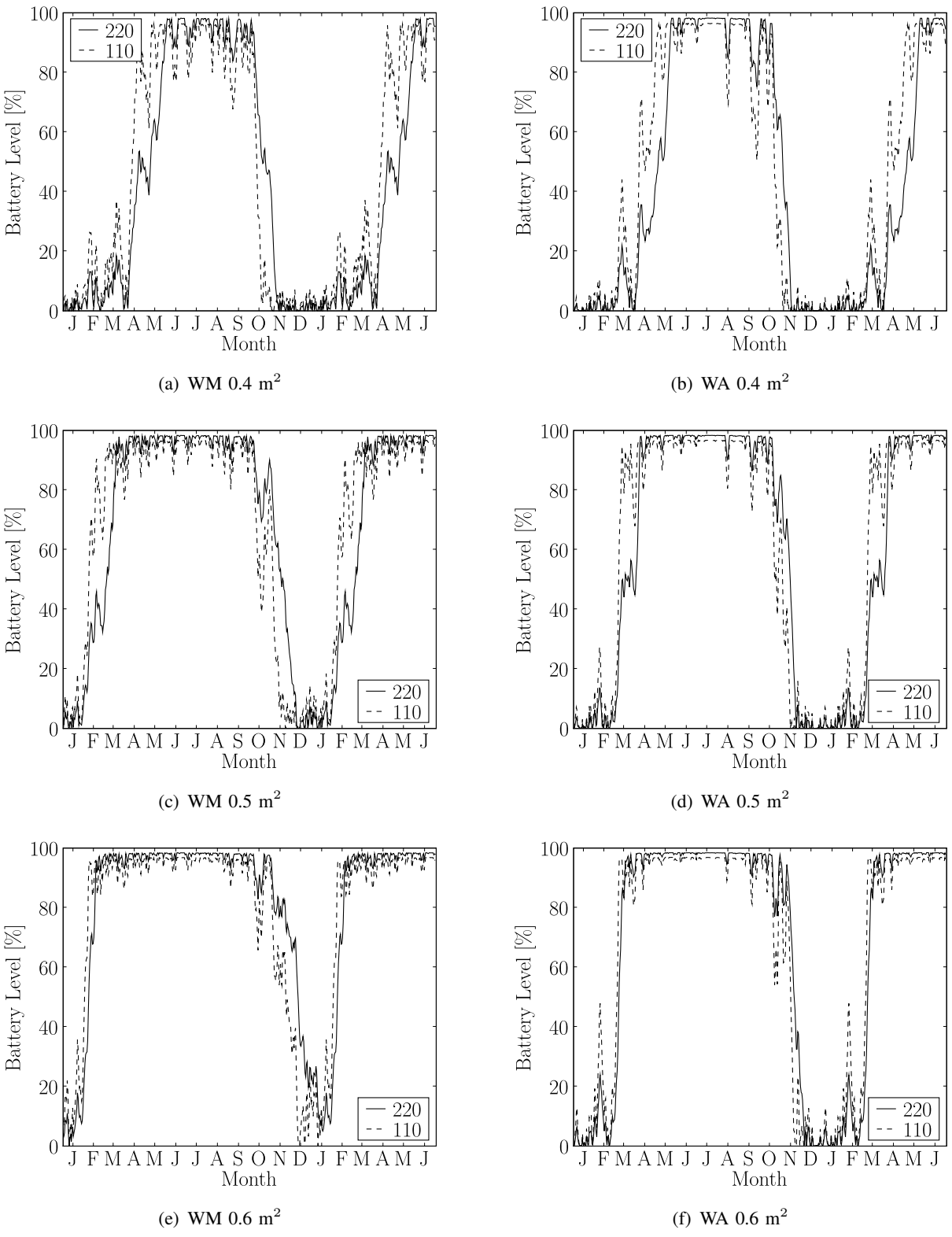

(a) WM 0.4 m^2

(b) WA 0.4 m^2

(c) WM 0.5 m^2

(d) WA 0.5 m^2

(e) WM 0.6 m^2

(f) WA 0.6 m^2

Fig. 19. Limited battery capacity experiment with varied panel size and battery capacity: Battery level in percentage capacity for two locations each with two battery capacities and three solar panel areas. Battery capacity is presented in percent capacity relative to the battery size (110 or 220 Ah). Panel size is 0.4, 0.5 or 0.6 m^2.

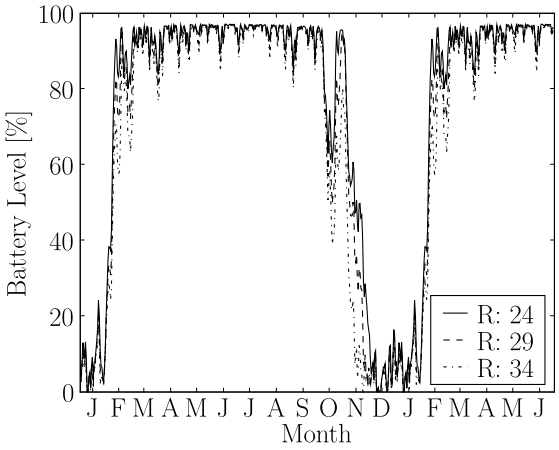

(a) Computer: 20 W

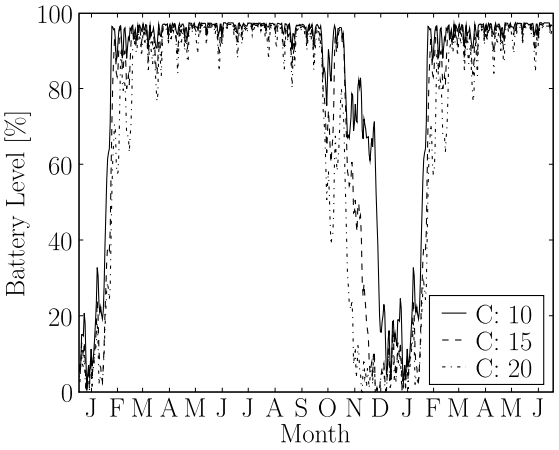

(b) Radar: 34 W

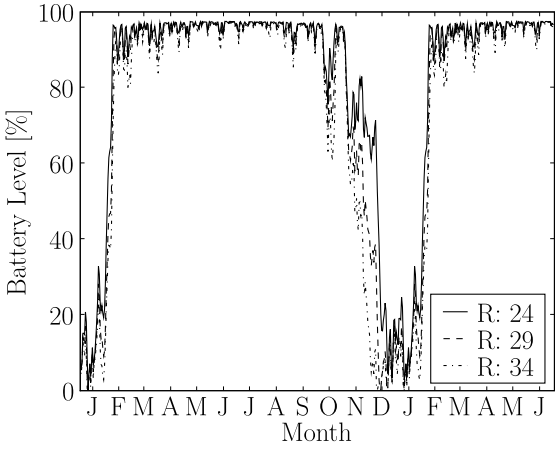

(c) Computer: 15 W

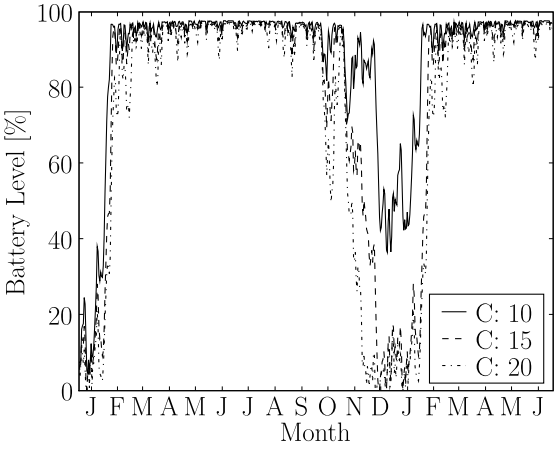

(d) Radar: 29 W

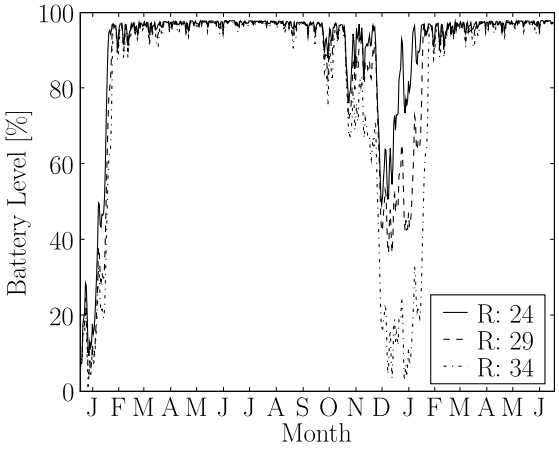

(e) Computer: 10 W

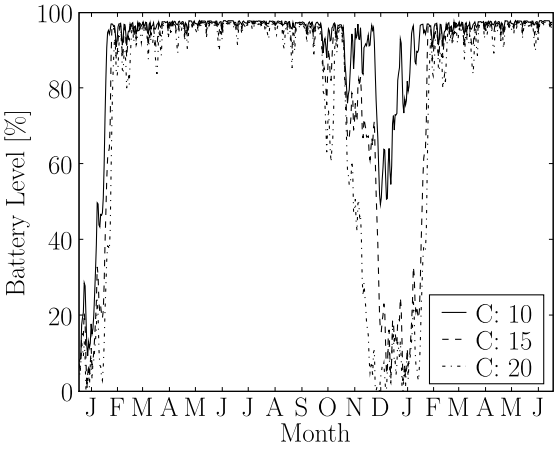

(f) Radar: 24 W

Fig. 20. Optimizing power consumption experiment: battery level in percentage capacity relative to a 110 Ah battery for 9 different system configurations. Radar or computer power consumption was reduced by 5 or 10 Watts.

range resulted in lower battery levels. As the range is reduced the number of hops and therefore number of network transmissions required to pass data through the network would increase. The reduction in range does not result in power savings in the sensing function as the power consumption for that function is fixed by the transmitter type.

The impact of network activity is illustrated by comparing the nodes with the maximum and minimum battery levels over the 18 month period. Figure 24 shows the nodes with the maximum and minimum battery levels for each of the networks while Figure 25 shows the total network traffic for those same nodes. These nodes for the WM case are indicated by the black and white dots in Figure 10. In most cases the node with the minimum battery was one hop from the sink node which was in the center of the network. While the nodes with the maximum battery was located on the edge of the network. This suggests that the energy hotspot is being caused by the forwarding of data for other nodes, following the funneling effect [25].

In the higher density networks the nodes with minimum battery level processed significantly more data than the nodes which had the maximum battery levels. Network activity can drain a considerable amount of energy. While the power consumption of the networking is small compared to the other components, the power consumed by the associated computing causes significant energy consumption. Figure 24 demonstrates that network activity may cause some nodes to fail. Network routing schemes such as LEACH [26] have been developed to adjust routes in wireless sensor networks based on energy consumption. Many of these routing algorithms are designed for the mote class of sensor network hardware and rely on the omni-directional signaling of the mote networks. Energy aware routing algorithms for fixed point to point networks will need to be identified or developed for OTG networks.

F. Conclusions

The OTGsim simulator may be used to investigate node and network parameters for large scale network deployments without the cost of those deployments. The simulator is being validated and refined using the smaller scale testbeds. The results of the simulations presented above demonstrate that the OTG radar concept is viable across the continental United States. Operation of the networks at higher latitudes will be limited during the winter months. Increasing the power generation sub-system will partially improve performance during the low power months but can not extend the operation to the full year. Higher density networks will suffer from network energy hot spots if fixed routing schemes are used.

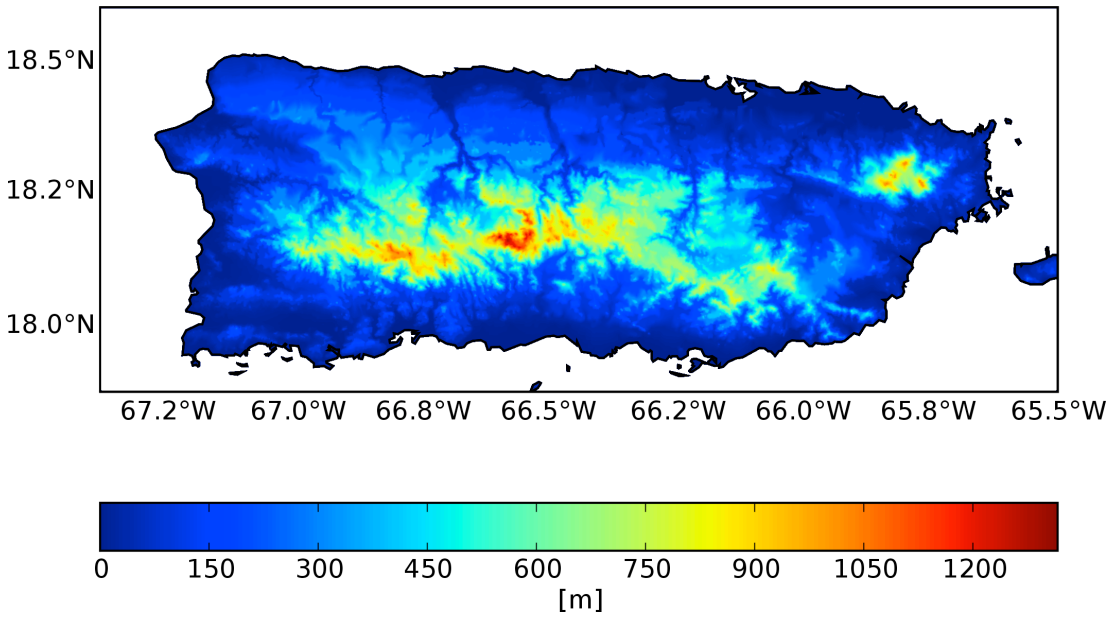

Fig. 21. Puerto Rico USGS Digital Elevation Model used to generated networks shown in Figure 22.

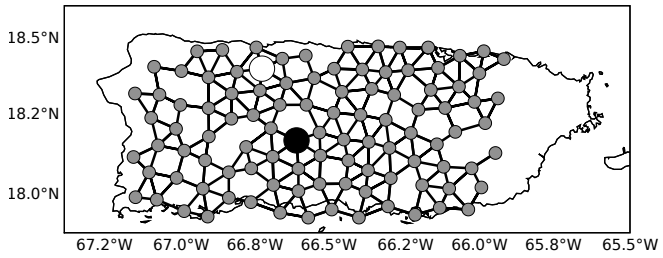

(a) 10 km spacing, 102 nodes

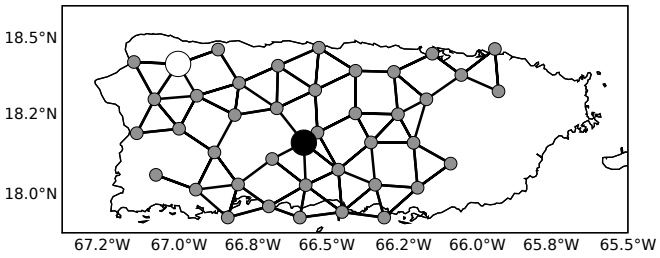

(b) 15 km spacing, 41 nodes

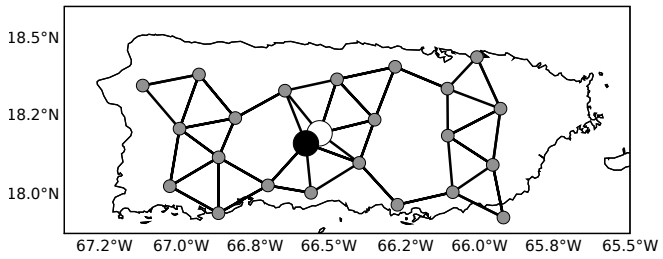

(c) 20 km spacing, 24 nodes

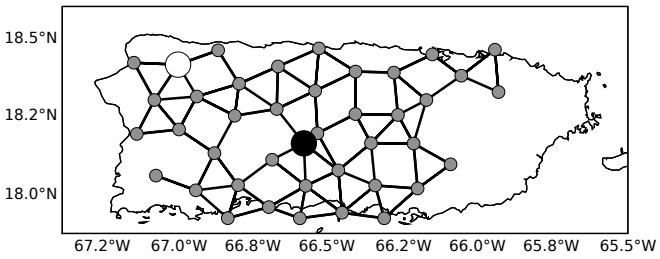

(d) 15 km spacing, 15 nodes

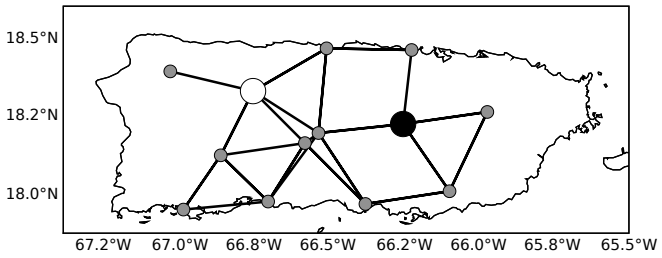

(e) 30 km spacing, 13 nodes

Fig. 22. Example networks for simulation at the Puerto Rico site. Dots indicate node location. White and black dots indicate nodes with minimum and maximum cumulative battery level as discussed in Section IV-E. Black lines indicate line of site communications link. The USGS DEM used to develop the networks is shown in Figure 21.

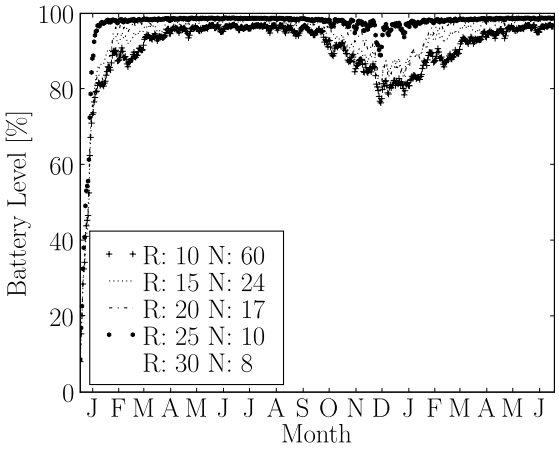

(a) WM Average Battery Level

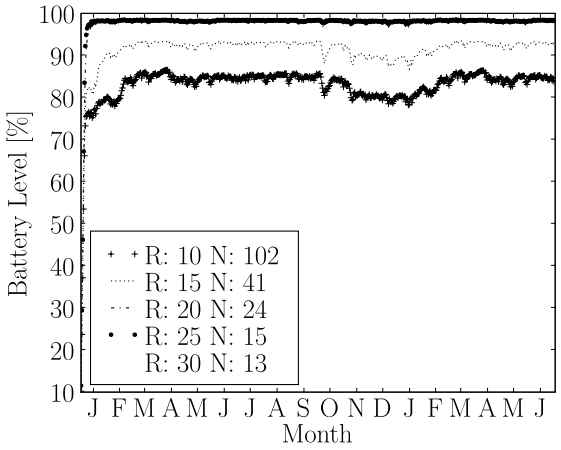

(b) PR Average Battery Level

Fig. 23. Node spacing experiment: average battery level for WM and PR, node separation was been varied from 10 - 30 km. The number of nodes in each network is indicated in the legend of the figure.

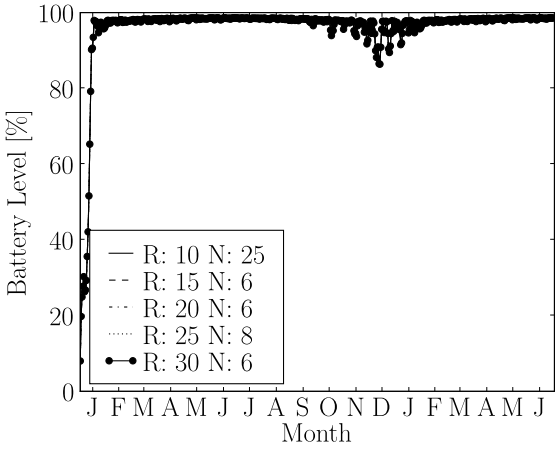

(a) WM Maximum

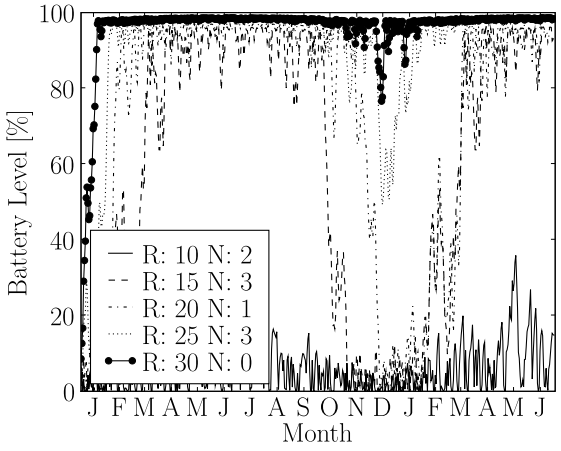

(b) WM Minimum

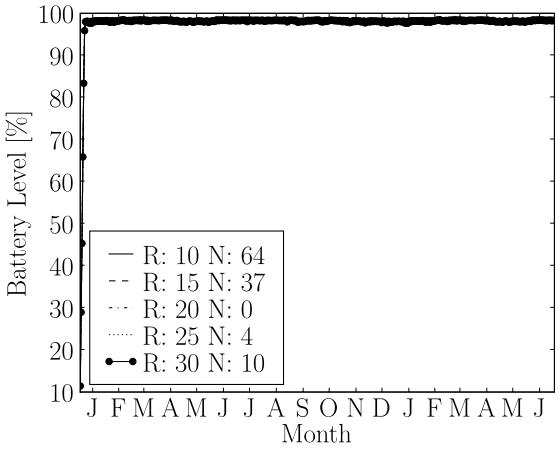

(c) PR Maximum

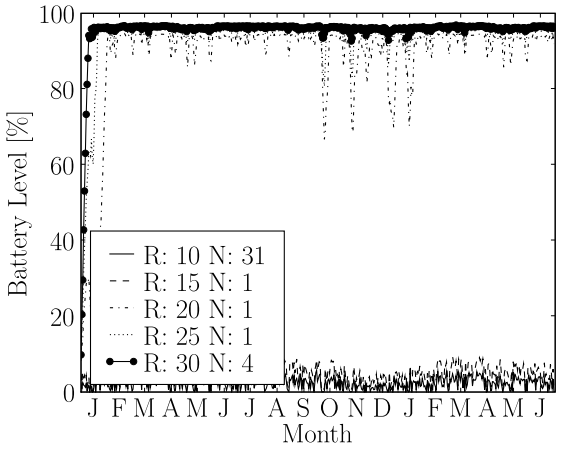

(d) PR Minimum

Fig. 24. Node spacing experiment: battery level of the nodes with the maximum and minimum cumulative sum battery levels. Label indicates range between nodes and the node id of maximum or minimum node.

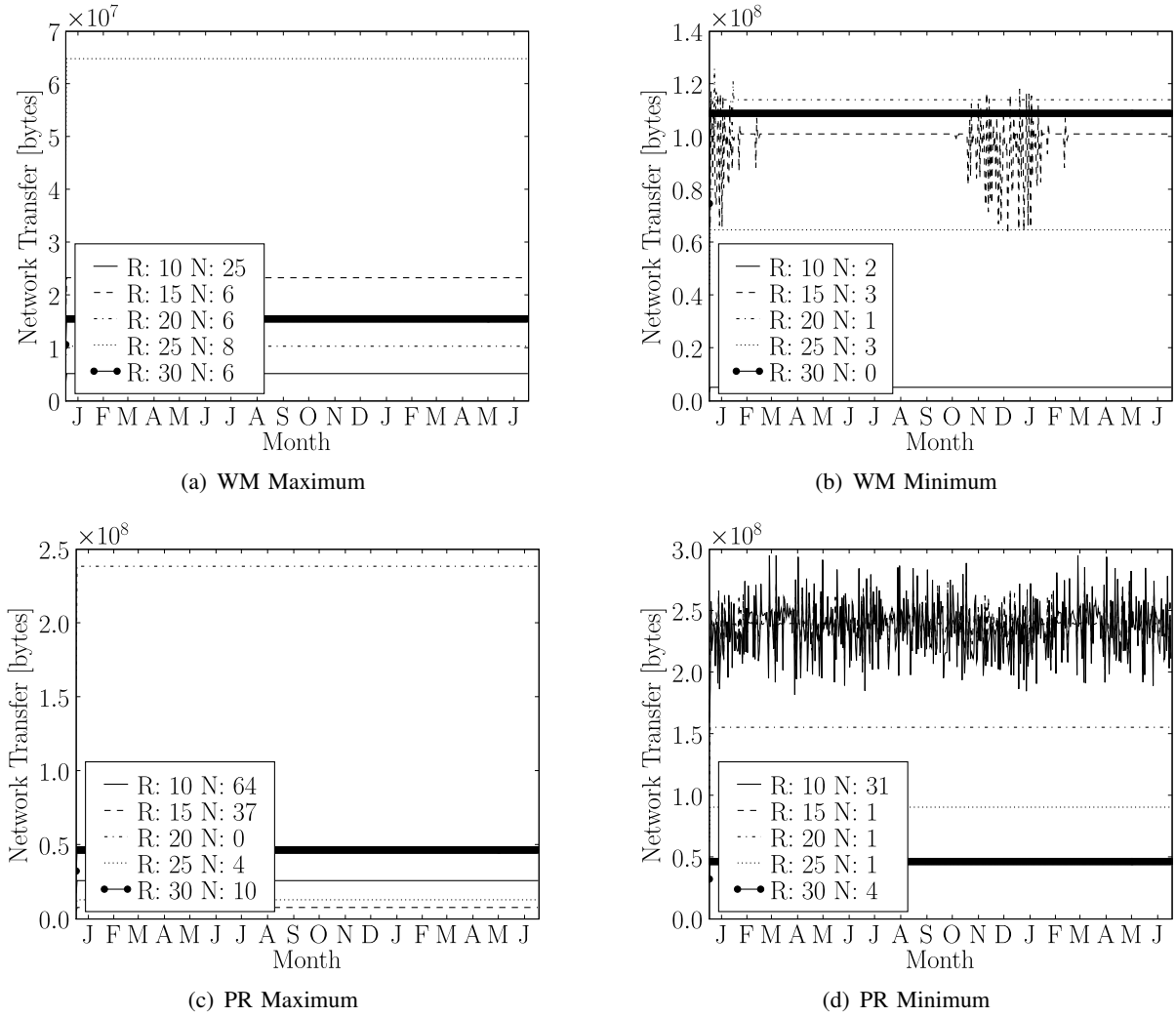

(a) WM Maximum

(b) WM Minimum

(c) PR Maximum

(d) PR Minimum

Fig. 25. Node spacing experiment: total network traffic, send and receive, of the nodes with maximum and minimum cumulative sum battery levels identified in Fig. 24.

APPENDIX

The solar power generation estimates presented in previous chapters are modeled using the U.S. National Renewable Energy Laboratory's Typical Meteorological Year 2 (TMY2) data set [18]. This data set provides a 30 year average of hourly solar and meteorological parameters. These parameters are provided for 239 sites across the continental United States and Puerto Rico (Figure **??**). Simulation of an OTG network uses the node locations to choose the geographically closest TMY2 site to be used for simulation. The global horizontal radiation, diffuse horizontal radiation, and snow coverage parameters are used in the estimation of the expected power generated by a solar panel. The global horizontal radiation is the total solar radiation incident on a horizontal surface. It is the sum of the beam horizontal radiation and the diffuse horizontal radiation. Beam radiation is solar radiation which has not been scattered by the Earth's atmosphere. Diffuse radiation has been scattered by the atmosphere before arriving at the solar panel. It has been assumed that the panel is at a fixed position and is pointed to face due south. The global horizontal radiation estimates are transformed to estimate the solar irradiation incident on the tilted panel following [20].

The ratio of beam radiation on a tilted surface to that on a horizontal surface is,

$$R_b = \frac{\cos\theta}{\cos\theta_z} \tag{2}$$

where θ is the *angle of incidence* between the panel and the sun, and θ_z is the *zenith angle* between a vertical line normal to the earth's surface and the sun. The zenith angle is the angle of incidence for a horizontal surface. It is,

$$\cos\theta_z = \cos\phi\cos\delta\cos\omega + \sin\phi\sin\delta \tag{3}$$

where ϕ is the panel latitude, ω is the *hour angle*, and δ is the *declination*. The solar declination δ, the angle between the sun and the Earth's equatorial plane, is,

$$\delta = 23.45\sin\left(\frac{360}{365}\left(n+284\right)\right)^{\circ} \tag{4}$$

where n is the day of the year ($n \in [0, 365]$). The hour angle is the angle east or west between the sun

Title	UTC Adjustment	Standard Longitude
Atlantic	-4	60° W
Eastern	-5	75° W
Central	-6	90° W
Mountain	-7	105° W
Pacific	-8	120° W

TABLE III
STANDARD LONGITUDES FOR STANDARD TIME ZONES COVERED BY THE TMY2 DATASET.

and the local meridian due to the rotation of the earth. It may be calculated as,

$$\omega = 15 * (\text{solar time} - 12) \tag{5}$$

where the solar time is,

$$\text{solar time} = \text{local time} + 4\,(L_{st} - L_{loc}) + E. \tag{6}$$

L_{st} is the standard meridian for the time zone and L_{loc} is the local longitude. The standard meridian for time zones covered by the TMY2 dataset is listed in Table III. E is the *equation of time*,

$$\begin{aligned} E = 229.2(7.5 \times 10^{-5} + 1.868 \times 10^{-3} \cos B - 3.2077 \times 10^{-2} \sin B - \\ 1.4615 \times 10^{-2} \cos 2B - 4.089 \times 10^{-2} \sin 2B) \end{aligned} \tag{7}$$

where B is,

$$B = (n-1)\,\frac{360}{365}\frac{\pi}{180}. \tag{8}$$

The equation of time is shown in Figure 26 and is in units of minutes. Finally, the angle of incidence for a tilted panel is,

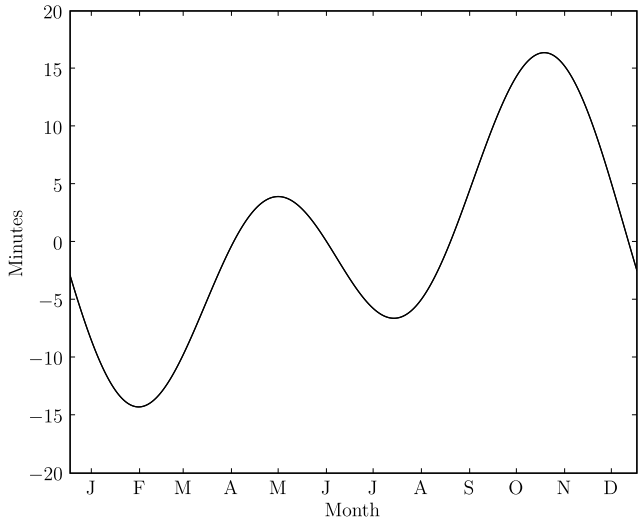

Fig. 26. Equation of time, adjustment to solar time over course of the year.

$$\begin{aligned}\cos\theta = &\sin\delta\sin\phi\cos\beta \\ &- \sin\delta\cos\phi\sin\beta\cos\gamma \\ &+ \cos\delta\cos\phi\cos\beta\cos\omega \\ &+ \cos\delta\sin\phi\sin\beta\cos\gamma\cos\omega \\ &+ \cos\delta\sin\beta\sin\gamma\sin\omega\end{aligned} \tag{9}$$

where β is the slope of the panel measured relative to the horizontal, γ is the azimuth angle of the panel (0° being due south), and ω_s is the sunset hour angle,

$$\cos\omega_s = -\tan\phi\tan\delta. \tag{10}$$

The angles listed in the preceding discussion are defined in Table IV.

Once the ratio of beam radiation on a tilted surface to that on a horizontal surface (Equation 2) has been calculated, the total radiation incident on the panel is,

$$I_T = I_b R_b + I_d\left(\frac{1-\cos\beta}{2}\right) + I\rho_g\left(\frac{1+\cos\beta}{2}\right) \tag{11}$$

where I_b is the direct horizontal beam radiation, I_d is the diffuse horizontal radiation, I is the total solar radiation incident on the horizontal surface, and ρ_g is the ground reflectance (taken to be 0.6 if the snow

	Name	Bounds	Definition
ϕ	Latitude	$[-90°, 90°]$	Latitude of panel.
δ	Declination	$[-23.45, 23.45°]$	Angular position of the sun at solar noon with respect to the plane of the equator, north positive.
β	Slope	$[0, 180°]$	Angle of panel relative to the horizontal.
γ	Surface azimuth angle	$[-180°, 180°]$	Azimuth angle of the panel with zero due south, east negative and west positive.
ω	Hour angle	$[-180°, 180°]$	Angle of the sun east or west of the local meridian due to rotation of the earth on its axis at 15° per hour, morning negative, afternoon positive.
θ	Angle of incidence	$[-90°, 90°]$	Angle between the beam radiation on a surface and the normal to the surface.
θ_z	Zenith angle	$[-90°, 90°]$	Angle between the vertical and the line to the sun; ie the angle of incidence of beam radiation on a horizontal surface.

TABLE IV
ANGLES USED IN SOLAR POWER GENERATION DISCUSSION.

depth is positive, 0.2 otherwise). This is the isotropic diffuse model of the sky. The first term accounts for the direct beam normal on the solar panel. The second term accounts for the diffuse radiation incident on the panel from the sky. The third term accounts for radiation reflected from the ground [20].

NEXRAD radar data from the National Climatic Data Center Data Archive [19] is used to simulate "workloads" for the OTG simulator. The archive data may be used to simulate the data that each radar in the network would observe. This may be used to evaluate dynamic control, network routing and data compression algorithms specific to the weather radar application. Level III [27] data may be downloaded from the NCDC Archive and converted to NetCDF format for use in the simulator. The data is converted using the NCDC Java NEXRAD Exporter [28]. The simulator currently uses the NEXRAD Level III Short Range (124 nm) Base Reflectivity data. Additional data types such as storm velocity may be added to the simulator in the future.

The simulator checks for the presence of NEXRAD data corresponding to the current simulation date and will automatically convert and load the data. The conversion process converts the data from the NEXRAD radial format to a raster format on a latitude and longitude grid. Data is selected for each OTG radar from the NEXRAD grid based on the simulated range. Original NEXRAD Level III reflectivity is shown in Figure 27, an individual OTG node sampled from the image, Figure 28, and the combined output of a 30 km OTG network, Figure 29. Figure 30 shows the ages of the samples in minutes when the sink image was produced. The simulator does not currently mask individual node data based on calculated line of sight.

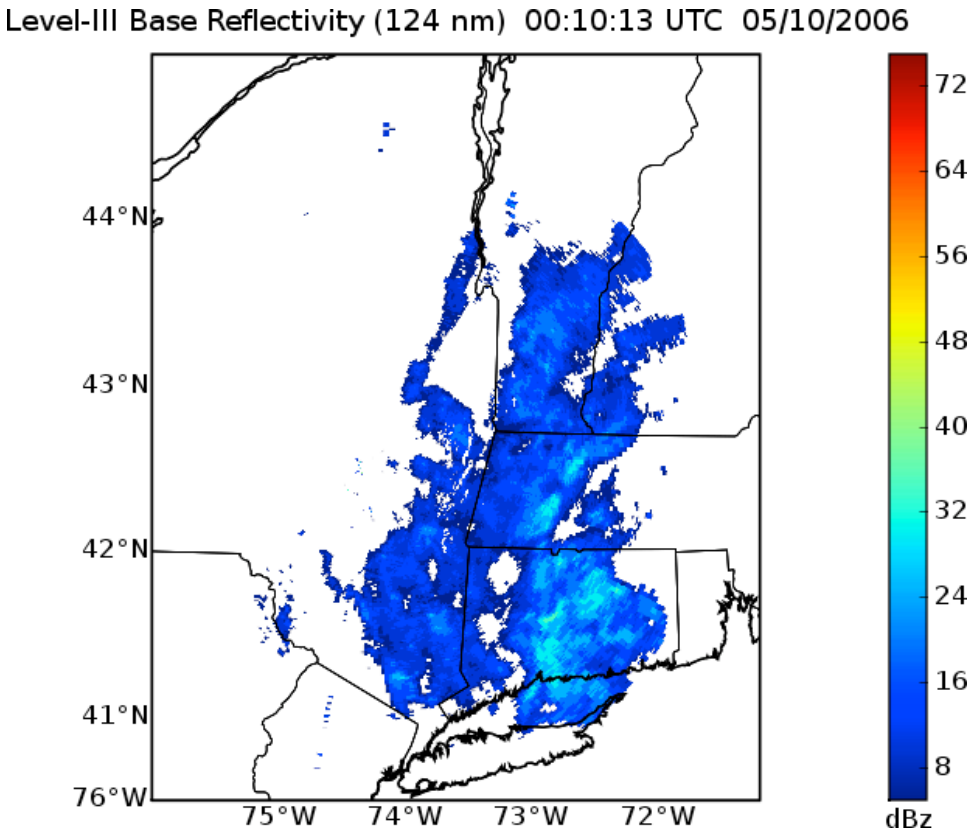

Fig. 27. Example NEXRAD Level-III Base Reflectivity.

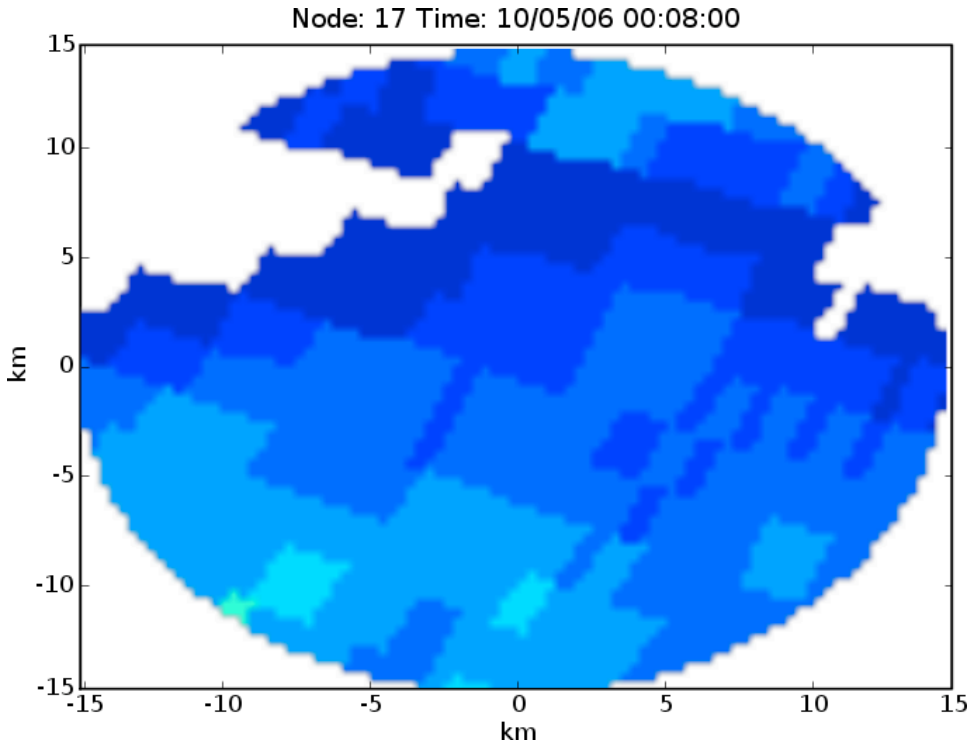

Fig. 28. Example individual OTG node sample from larger NEXRAD image shown in Figure 27.

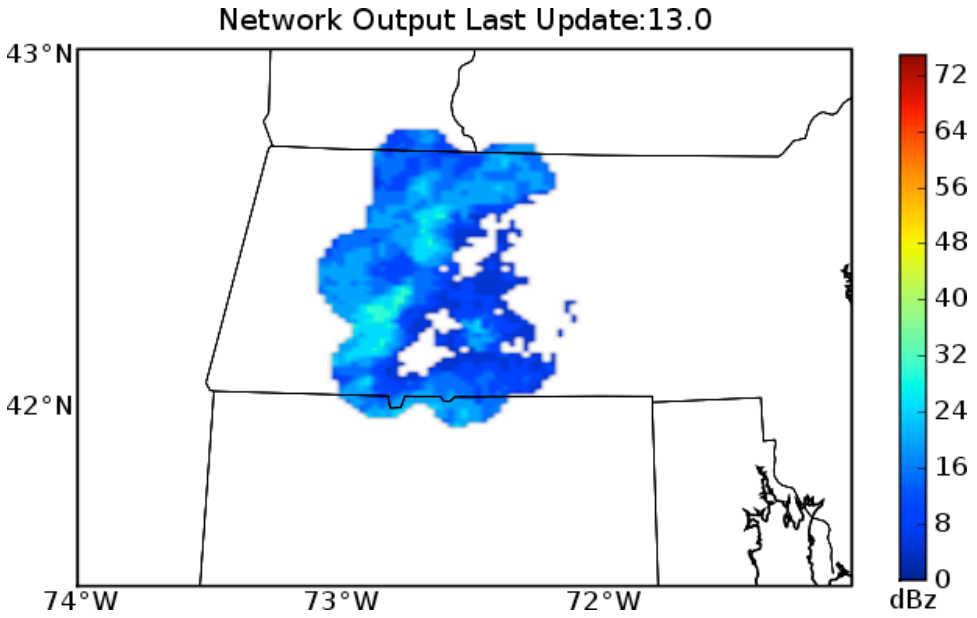

Fig. 29. OTG Network output at sink. Simulation used a 15 km spacing network shown in Figure10(c).

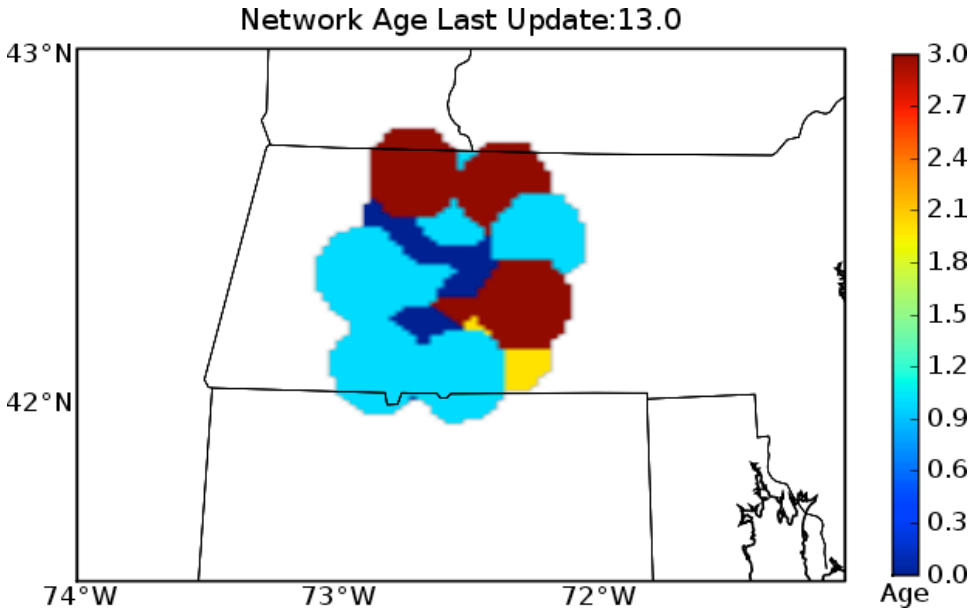

Fig. 30. Age in minutes of OTG samples (shown Figure 29) when received at sink node.

REFERENCES

[1] D. J. McLaughlin, V. Chandrasekar, K. Droegemeier, S. Fraiser, J. Kurose, F. Junyent, B. Philips, S. Cruz-Pol, and J. Colom, "Distributed Collaborative Adaptive Sensing (DCAS) for Improved Detection, Understanding, and Predicting of Atmospheric Hazards," in *Ninth Symposium on Integrated Observing and Assimilation Systems for the Atmosphere, Oceans, and Land Surface*. San Diego, CA: AMS, 2005.

[2] B. C. Donovan, D. J. McLaughlin, V. Chandrasekar, and J. Kurose, "Principles and Design Considerations for Short-Range Energy Balanced Radar Networks," in *International Geoscience and Remote Sensing Symposium*, Seoul, Korea, 2005.

[3] B. C. Donovan, D. J. McLaughlin, M. Zink, and J. Kurose, "Simulation of minimal infrastructure short-range radar netowrks," in *International Geoscience and Remote Sensing Symposium*, Barcelona, Spain, 2007.

[4] Q. Wang and W. Yang, "Energy Consumption Model for Power Management in Wireless Sensor Networks," in *Proceedings of the IEEE SECON Conference, San Diego, CA, USA*, Jun. 2007.

[5] V. Raghunathan, A. Kansal, J. Hsu, J. Friedman, and M. Srivastava, "Design considerations for solar energy harvesting wireless embedded systems," in *IEEE International Conference on Information Processing in Sensor Networks*, April 2005.

[6] C. M. Vigorito, D. Ganesan, and A. G. Barto, "Adaptive Control of Duty Cycling in Energy-Harvesting Wireless Sensor Networks," in *Proceedings of the IEEE SECON Conference, San Diego, CA, USA*, Jun. 2007.

[7] A. Kansal, J. Hsu, S. Zahedi, and M. B. Srivastava, "Power management in energy harvesting sensor networks," *ACM Transactions on Embedded Computing Systems*, vol. 6, no. 4, Sep. 2007.

[8] L. Pedersen, N. E. Jensen, and H. Madsen, "Network architecture for small x-band weather radars - test bed for automatic inter-calibration and nowcasting," in *33rd AMS Conference on Radar Meteorology*, August 2007.

[9] G. J. Pottie and W. J. Kaiser, "Wireless integrated network sensors," *Communications of the ACM*, vol. 43, no. 5, pp. 51–58, May 2000.

[10] C. Chong and S. Kumar, "Sensor networks: evolution, opportunities, and challenges," *Proceedings of the IEEE*, vol. 91, no. 8, August 2003, DOI: 10.1109/JPROC.2003.814918.

[11] K. Romer and F. Mattern, "The design space of wireless sensor networks," *IEEE Wireless Communications*, vol. 11, no. 6, pp. 54–61, Dec 2004.

[12] R. Woodbury, "Justification for Use of Photovoltaic Solar Panels with Battery Storage," University of Massachuesetts Amherst, Tech. Rep., 2004.

[13] *EPIA-MII Mini-ITX Mainboard Users Manual*, VIA Technologies, January 2004, version: 1.30.

[14] *NuDAQ PCI-9812/10 20MHz Simultaneous 4-CH Analog Input Card Users Manual*, Adlink Technology, Inc., March 2005, rev. 3.00.

[15] *ORiNOCO 11b/g PC Card*, Proxim Wireless Corporation, http://www.proxim.com/learn/library/datasheets/11bgpccard.pdf, Cited: April 20, 2006.

[16] R. J. Doviak and D. S. Zirić, *Doppler Radar and Weather Observations*, 2nd ed. Academic Press, 1993.

[17] *Simulation in Python*, SimPy Developer Team, http://simpy.sourceforge.net/, Cited: September 25, 2007.

[18] W. Marion and W. Urban, *User's Manual for TMY2s*, http://rredc.nrel.gov/solar/old_data/nsrdb/tmy2/, 1995, Cited: April 27, 2007.

[19] *NCDC NEXRAD Data Inventory*, U.S. Department of Commerce, National Climatic Data Center, http://www.ncdc.noaa.gov/nexradinv/, Cited: September 20, 2007.

[20] J. A. Duffie and W. A. Beckman, *Solar Engineering of Thermal Processes*, 2nd ed. Wiley, 1991.

[21] J. F. Kurose and K. W. Ross, *Computer Networking: a top-down approach featuring the Internet*, 2nd ed. Addison-Wesley, 2003.

[22] R. Patra, S. N. Sergiu amd Surana, A. Sheth, L. Subramanian, and E. Brewer, "Wildnet: Design and implementation of high performance wifi based long distance networks," *4th USENIX Symposium on Networked Systems Design & Implementation*, Feb 2007.

[23] *Standards for Digital Elevation Models*, U.S. Department of the Interior, U.S. Geological Survey, http://rockyweb.cr.usgs.gov/nmpstds/demstds.html, Cited: June 5, 2007.

[24] *USGS 1:250,000 DEM FTP Archive*, U.S. Department of the Interior, U.S. Geological Survey, http://edcftp.cr.usgs.gov/pub/data/DEM/250/, Cited: June 5, 2007.

[25] C.-Y. Wan, A. T. Campbell, and J. Crowcroft, "A case for all-wireless, dual-radio virtual sinks," in *SenSys '04: Proceedings of the 2nd international conference on Embedded networked sensor systems*. New York, NY, USA: ACM, 2004, pp. 267–268.

[26] W. R. Heinzelman, A. Chandrakasan, and H. Balakrishnan, "Energy-efficient communication protocol for wireless microsensor networks," in *Proceedings of the Hawaii International Conference on System Sciences*, 2000.

[27] *Federal Meteorological Handbook No. 11 Doppler Radar Meteorlogical Observations Part A*, Fcm-h11a-2006 ed., U.S. Derpartment Of Commerce/ National Oceanic and Atmospheric Administration Office of the Federal Coordinator For Meteorlogical Services and Supporting Research.

[28] "NCDC Java Nexrad Tools." [Online]. Available: http://www.ncdc.noaa.gov/oa/radar/jnx/jnt-batch.php